

(12)

AD A11 9984

TECHNICAL

DTIC FILE COPY

TN NO: N-1628

TITLE: WIND-INDUCED STEADY LOADS ON SHIPS

AUTHOR: R. Owens and P. Palo

DATE: April 1982

SPONSOR: Naval Facilities Engineering Command

PROGRAM NO: YF59.556.091.01.403

# NOTE

NAVAL CIVIL ENGINEERING LABORATORY  
PORT HUENEME, CALIFORNIA 93043

Approved for public release; distribution unlimited.

DTIC  
ELECTE  
OCT 7 1982  
S H D

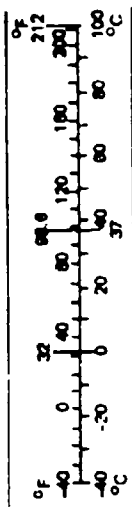
82 10 07 011

METRIC CONVERSION FACTORS

Approximate Conversions to Metric Measures		Approximate Conversions from Metric Measures	
When You Know	Multiply by	To Find	Symbol
<b>LENGTH</b>			
inches	2.5	centimeters	cm
feet	30	centimeters	cm
yards	0.9	meters	m
miles	1.6	kilometers	km
<b>AREA</b>			
square inches	6.5	square centimeters	cm <sup>2</sup>
square feet	0.09	square meters	m <sup>2</sup>
square yards	0.8	square meters	m <sup>2</sup>
square miles	2.6	square kilometers	km <sup>2</sup>
acres	0.4	hectares	ha
<b>MASS (weight)</b>			
ounces	28	grams	g
pounds	0.45	kilograms	kg
short tons (2,000 lb)	0.9	tonnes	t
<b>VOLUME</b>			
teaspoons	5	milliliters	ml
tablespoons	15	milliliters	ml
fluid ounces	30	milliliters	ml
oz	0.24	liters	l
pints	0.47	liters	l
quarts	0.95	liters	l
gallons	3.8	liters	l
cubic feet	0.03	cubic meters	m <sup>3</sup>
cubic yards	0.76	cubic meters	m <sup>3</sup>
<b>TEMPERATURE (exact)</b>			
Fahrenheit temperature	5/9 (after subtracting 32)	Celsius temperature	°C

\*1 in. = 2.54 (exact). For other exact conversions and more detailed tables, see NBS Misc. Publ. 288, Units of Weights and Measures, Price \$7.25, SD Catalog No. C-13.10-288.

When You Know	Multiply by	To Find	Symbol
<b>LENGTH</b>			
millimeters	0.04	inches	in
centimeters	0.4	inches	in
meters	3.3	feet	ft
meters	1.1	yards	yd
kilometers	0.6	miles	mi
<b>AREA</b>			
square centimeters	0.16	square inches	in <sup>2</sup>
square meters	1.2	square yards	yd <sup>2</sup>
square kilometers	0.4	square miles	mi <sup>2</sup>
hectares (10,000 m <sup>2</sup> )	2.5	acres	ac
<b>MASS (weight)</b>			
grams	0.035	ounces	oz
kilograms	2.2	pounds	lb
tonnes (1,000 kg)	1.1	short tons	st
<b>VOLUME</b>			
milliliters	0.03	fluid ounces	fl oz
liters	2.1	pints	pt
liters	1.06	quarts	qt
liters	0.26	gallons	gal
cubic meters	35	cubic feet	ft <sup>3</sup>
cubic meters	1.3	cubic yards	yd <sup>3</sup>
<b>TEMPERATURE (exact)</b>			
Celsius temperature	9/5 (then add 32)	Fahrenheit temperature	°F



Unclassified

SECURITY CLASSIFICATION OF THIS PAGE (When Data Entered)

REPORT DOCUMENTATION PAGE		READ INSTRUCTIONS BEFORE COMPLETING FORM
1. REPORT NUMBER TN-1628	2. GOVT ACCESSION NO. AD-A119984	3. RECIPIENT'S CATALOG NUMBER
4. TITLE (and Subtitle)  WIND-INDUCED STEADY LOADS ON SHIPS		5. TYPE OF REPORT & PERIOD COVERED Not final; Oct 1980 - Jun 1981
		6. PERFORMING ORG. REPORT NUMBER
7. AUTHOR(s)  R. Owens and P. Palo		8. CONTRACT OR GRANT NUMBER(s)
9. PERFORMING ORGANIZATION NAME AND ADDRESS NAVAL CIVIL ENGINEERING LABORATORY Port Hueneme, California 93043		10. PROGRAM ELEMENT PROJECT, TASK AREA & WORK UNIT NUMBERS 62759N; YF59.556.091.01.403
11. CONTROLLING OFFICE NAME AND ADDRESS Naval Facilities Engineering Command Alexandria, Virginia 22332		12. REPORT DATE April 1982
		13. NUMBER OF PAGES 55
14. MONITORING AGENCY NAME & ADDRESS (if different from Controlling Office)		15. SECURITY CLASS. (of this report)  Unclassified
		15a. DECLASSIFICATION DOWNGRADING SCHEDULE
16. DISTRIBUTION STATEMENT (of this Report)  Approved for public release; distribution unlimited.		
17. DISTRIBUTION STATEMENT (of the abstract entered in Block 20, if different from Report)		
18. SUPPLEMENTARY NOTES		
19. KEY WORDS (Continue on reverse side if necessary and identify by block number)  Wind forces, moorings, ships.		
20. ABSTRACT (Continue on reverse side if necessary and identify by block number)  Methods are presented for predicting the lateral and longitudinal steady wind drag forces and yaw moment versus incident wind angle for various ship types. These methods were developed based on experimental model data for 31 ships compiled from six independent tests. Except for hull-dominated ships, which are considered separately, the longitudinal wind drag force is computed using a constant headwind coefficient that has an accuracy of  (continued)		

DD FORM 1473

1 JAN 73

EDITION OF 1 NOV 65 IS OBSOLETE

Unclassified

SECURITY CLASSIFICATION OF THIS PAGE (When Data Entered)

Unclassified

SECURITY CLASSIFICATION OF THIS PAGE(When Data Entered)

20. Continued

12%. This coefficient can be modified depending on the ship type and above deck features. Over the remainder of the incident wind directions the coefficient is based on curve fits to the data. The lateral force coefficient is also derived from a curve fitted to the data and is based on a peak value with a 10% deviation; the coefficient is dependent on mean heights and projected areas of the hull and superstructure. Determination of the recommended moment response is based on an inspection and interpolation of existing experimental data. Recommendations from other investigations are also presented for comparison, and a sample problem is included.

Library Card

Naval Civil Engineering Laboratory  
WIND-INDUCED STEADY LOADS ON SHIPS, by R. Owens and  
P. Palo  
TN-1628 55 pp illus April 1982 Unclassified

1. Wind drag force 2. Yaw moment response I. YF59.556.091.01.403

Methods are presented for predicting the lateral and longitudinal steady wind drag forces and yaw moment versus incident wind angle for various ship types. These methods were developed based on experimental model data for 31 ships compiled from six independent tests. Except for hull-dominated ships, which are considered separately, the longitudinal wind drag force is computed using a constant headwind coefficient that has an accuracy of 12%. This coefficient can be modified depending on the ship type and above deck features. Over the remainder of the incident wind directions the coefficient is based on curve fits to the data. The lateral force coefficient is also derived from a curve fitted to the data and is based on a peak value with a 10% deviation; the coefficient is dependent on mean heights and projected areas of the hull and superstructure. Determination of the recommended moment response is based on an inspection and interpolation of existing experimental data. Recommendations from other investigations are also presented for comparison, and a sample problem is included.

Unclassified

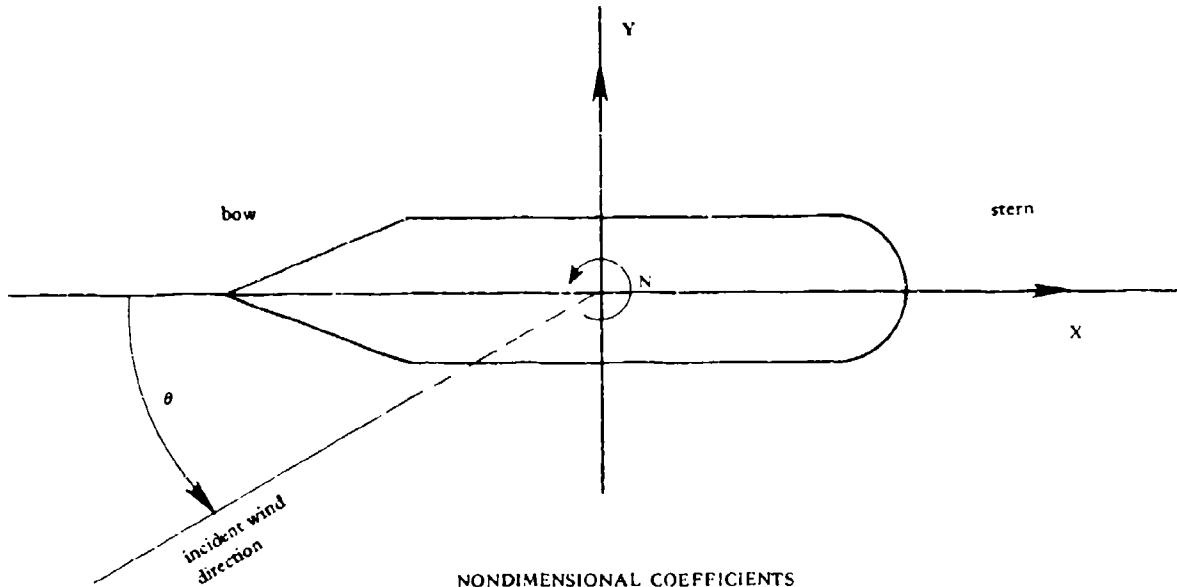
SECURITY CLASSIFICATION OF THIS PAGE(When Data Entered)

## CONTENTS

	Page
INTRODUCTION . . . . .	1
EXPERIMENTAL DATA . . . . .	2
SUMMARY OF WIND FORCE EQUATIONS . . . . .	3
Lateral Wind Force . . . . .	3
Longitudinal Wind Force . . . . .	4
Wind Moment . . . . .	7
DEVELOPMENT OF PROCEDURE . . . . .	7
Wind Gradient . . . . .	7
Lateral Wind Force . . . . .	8
Lateral Wind Shape Function . . . . .	10
Longitudinal Wind Force . . . . .	11
Wind Yaw Moment . . . . .	13
ATYPICAL SHIP TYPES . . . . .	15
DISCUSSION OF RECOMMENDED PROCEDURES . . . . .	16
Comparisons to Experimental Data . . . . .	16
Comparison to Other Investigators . . . . .	17
CONCLUSIONS AND RECOMMENDATIONS . . . . .	18
ACKNOWLEDGMENT . . . . .	18
REFERENCES . . . . .	18
NOMENCLATURE . . . . .	21
APPENDIX - Sample Problem . . . . .	47

DTIC  
COPY  
INSPECTED  
2

Accession For	
GRA&I	<input checked="" type="checkbox"/>
TAB	<input type="checkbox"/>
Announced	<input type="checkbox"/>
Classification	
Distribution/	
Availability Codes	
Dist	Avail and/or
	Special
A	



NONDIMENSIONAL COEFFICIENTS

$C_X$  = longitudinal force coefficient

$C_Y$  = lateral force coefficient

$C_N$  = yaw moment coefficient

$$0^\circ < \theta < 180^\circ$$

Positive Wind Load Conventions  
and Coordinate System

## INTRODUCTION

One major source of error in the design of mooring systems for large ships has been the lack of accurate knowledge of wind loads. Many of the present methods for calculating these loads are unreliable or cumbersome to use. One method, proposed primarily for its simplicity, is presented in the chapter 7 revision of the NAVFAC Design Manual DM-26 (Ref 1). This method involves three curves that are used for the lateral, longitudinal, and moment loads for all ships. However, experimental data have shown this approach to be too approximate for general application.

The purpose of this document is to describe an improved method for computing accurately and easily the wind drag forces, by taking gross individual ship characteristics into account. Results of this investigation are applicable primarily to "typical" ships, although some of the 31 models used were not typical. Even so, an effort was made to present trends and recommendations for "atypical" ships by using their collected responses to better define the wind load characteristics of unique ships and to amplify coefficient trends for the more typical ships.

In many cases accurate data regarding projected and other surface areas of the models are lacking. For this reason, along with the fact that scale model behavior is often not completely representative of full scale ship behavior (surface roughness, railings, etc.), the accuracy of the experimental results is not above question. Care was taken to establish the reliability and accuracy of all experimental results by comparing projected model areas to a variety of sources and by comparing results of independent tests for similar ships.

Because of the complex superstructure geometry on most ships, the lateral and longitudinal wind forces can be calculated more directly than the moment. The emphasis of this note is, therefore, placed on the accurate determination of these two forces, while the moment response is

only observed for trends. The effect of the naturally occurring wind gradient has also been incorporated into this analysis, especially for the case of the lateral wind force, where the projected ship area is greatest.

This analysis was undertaken because of the concern for reliable ship load files (for wind and current loads) expressed in Reference 2 and deals only with the wind load aspect. The design procedures developed here are particularly useful for mooring analysis problems in protected harbors, where wave and current loads are usually small. This work was performed as part of the effort on Mooring Systems Prediction Techniques within the Ocean Facilities Engineering Exploratory Development Program, sponsored by the Naval Facilities Engineering Command.

#### EXPERIMENTAL DATA

The experimental data used in this investigation were taken from six independent sources (Refs 3 through 8); data on 31 ship models were used from the available 40 models. The data not used were those considered to be from unconventional models or those lacking information in some respect. Also, only data on 2 ship models were used from Reference 7 because the data are considered by many to be too conservative. Of the 31 models used: 18 were tankers and cargo ships, including 4 center island tankers; 3, aircraft carriers; 2, cruisers; 1, a destroyer, which was independently tested by two sources; 2, passenger liners; and the remaining 5, general class.

Data from 19 of these 31 models were used for the  $C_x$  coefficient determination and 13 for the  $C_y$  coefficient determination because not all sources used a wind gradient in the experiment, and because the main concern of this investigation was with tankers and cargo ships; there were less data on warships. From these data, a more reliable method for calculating wind loads than that given by the three reference curves presented in Reference 1 and illustrated in Figure 1 was developed

Approximate silhouettes for some of these ships are presented in Figure 2 to allow the reader to associate the recommendations from this report with the various ship types.

#### SUMMARY OF WIND FORCE EQUATIONS

Equations for the lateral and longitudinal forces versus incident wind angle are presented in this section. Derivations and a discussion are presented in later sections. It should be stated that these forces are actually dependent on Reynolds Number, which is assumed for typical ships to be large enough to allow for constant coefficients. The general equation for these forces can be expressed as follows:

$$F = \frac{1}{2} \rho V^2 A C f(\theta) \quad (1)$$

where;

- F = wind force,  $F_X$  or  $F_Y$ ; or yaw moment, N
- $\rho$  = density of air
- V = relative wind velocity with respect to ship
- A = projected ship area,  $A_X$  (used for  $F_X$ ); or  $A_Y$  (used for  $F_Y$ ); or  $A_Y L$  used for N,  $L \hat{=}$  ship length
- C = dimensionless wind drag coefficient,  $C_X$ ,  $C_Y$ , or  $C_N$
- $f(\theta)$  = normalized shape function dependent on incident wind angle ( $\theta$ )

#### Lateral Wind Force

The following results have been obtained for the lateral wind drag coefficient ( $C_Y$ ) by summing forces obtained for the hull and superstructure:

$$C_Y = \frac{C_{YC} \left[ \left( \frac{\bar{v}_S}{V_R} \right)^2 A_S + \left( \frac{\bar{v}_H}{V_R} \right)^2 A_H \right]}{A_Y} \quad (2)$$

where the terms  $(\bar{v}_S/V_R)$  and  $(\bar{v}_H/V_R)$  are the average wind velocities over the superstructure and the hull, respectively, taken from a normalized wind gradient curve presented in Figure 3.  $C_{YC}$  was determined from the available experimental data and was calculated to be:

$$C_{YC} = 0.92 \pm 0.1$$

The following recommended normalized shape function was fitted to the available data:

$$f(\theta) = \frac{\sin \theta - \sin (5\theta)/20}{1 - 1/20} \quad (3)$$

This function is illustrated in Figure 4.

#### Longitudinal Wind Force

The longitudinal wind force calculations are not as straightforward as the lateral force calculations. Both the coefficient and shape function vary according to ship type and characteristics.

Selection of Longitudinal Force Coefficient ( $C_X$ ). In general, vessels are classified as either hull dominated, (such as aircraft carriers and passenger liners) or normal (such as warships, tankers). Second, due to possible asymmetry of the superstructure relative to midships, separate coefficients are used for headwind and tailwind loadings, designated as  $C_{XB}$  and  $C_{XS}$ , respectively.

For hull dominated vessels, the following is recommended:

$$C_{XB} = C_{XS} = 0.40$$

For all remaining types of ships, except for specific deviations, the following are recommended:

$$C_{XB} = 0.70$$

$$C_{XS} = 0.60$$

Deviations to these general coefficients are listed below. First, for center island tankers only, an increased headwind coefficient is recommended:

$$C_{XB} = 0.80$$

For ships with an excessive amount of superstructure, such as destroyers and cruisers:

$$C_{XS} = 0.80$$

A universal adjustment of 0.08 is also recommended for all cargo ships and tankers with cluttered decks (i.e., masts, booms, piping, and other substantial obstructions). This would apply to both  $C_{XB}$  and  $C_{XS}$ .

Selection of the Longitudinal Shape Function ( $f(\theta)$ ). As with the longitudinal coefficient, two distinct longitudinal shape functions are recommended that differ over the headwind and tailwind regions. These regions are separated by the incident wind angle that produces no net longitudinal force, designated  $\theta_2$  for zero crossing. Selection of  $\theta_2$  is determined by the mean superstructure location relative to midships (MS):

Just forward of MS:	$\theta_2 = 80$ degrees
on MS:	$\theta_2 = 90$ degrees
aft of MS:	$\theta_2 = 100$ degrees
Hull dominated:	$\theta_2 = 120$ degrees

Generally,  $\theta_2 \sim 100$  degrees seems typical for many ships, including center island tankers, while  $\theta_2 \sim 110$  degrees is recommended for warships.

For ships with single, distinct superstructures and for hull dominated ships, the following longitudinal shape function is recommended:

$$f(\theta) = \cos \phi \quad (4)$$

where

$$\phi = \left( \frac{90}{\theta_z} \right) \theta \quad \text{for } \theta < \theta_z \quad (5)$$

$$\phi = \left( \frac{90}{180 - \theta_z} \right) (\theta - \theta_z) + 90 \quad \text{for } \theta > \theta_z$$

Examples of ships in this category, as illustrated in Figure 2, are: all aircraft carriers, EC-2, Cargos A, C, and E. These shape functions are shown in Figure 5 for  $\theta_z = 90$  degrees.

Ships with distributed superstructure fall into the second shape function category called "humped cosine." With these ships the longitudinal force actually increases with oblique wind angles (up to 30 degrees) as additional superstructure is exposed to the wind. For these ships, the following shape function is recommended:

$$f(\theta) = \frac{\sin \gamma - (\sin 5 \gamma)/10}{1 - 1/10} \quad (6)$$

with

$$\gamma = \left( \frac{90}{\theta_z} \right) \theta + 90 \quad \theta < \theta_z \quad (7)$$

$$\gamma = \left( \frac{90}{180 - \theta_z} \right) \theta + \left( 180 - \frac{90 \theta_z}{180 - \theta_z} \right) \quad \theta > \theta_z \quad (8)$$

Notice the similarity between Equation 3 used for the lateral force and Equation 6 used for the longitudinal force. Examples of ships in this second category, illustrated in Figure 2, include: destroyers, cruisers, Meteor, and T-AO tanker. This shape function is developed under the PROCEDURE section, and is illustrated as part of a family of shapes in Figure 6.

## Wind Moment

For the general moment response tendencies of a ship, refer to Figure 7. More specific moment coefficient curves are presented in Figures 8 through 14 for the various ship types considered. More details concerning the moment response are provided in the DEVELOPMENT OF PROCEDURE section.

## DEVELOPMENT OF PROCEDURE

### Wind Gradient

The two major factors that directed the approach of this investigation were: quantifying the effects of the natural wind gradient over the ship profile, and allowing for more individualized shape functions based on vessel characteristics.

The wind gradient is obtained from the following equation (Ref 9):

$$\frac{v}{v_R} = \left( \frac{h}{h_R} \right)^{\frac{1}{n}} \quad (9)$$

where,

$\frac{v}{v_R}$  = normalized wind velocity at height (h)

h = height above free surface

$h_R$  = constant reference height

n = arbitrary exponent

For the purposes of this report, the reference height ( $h_R$ ) is taken as 33 feet (10 meters) above the mean sea surface, and the exponent (n) is assumed to be 7. It was determined that the value of n is not critical, since no significant difference was observed in the calculated wind drag

forces when n was varied from 5 to 10; the value of n = 7 is chosen primarily because it is the value most commonly used for this type of application (Ref 10).

In dealing with the wind gradient, the hull and superstructure of each vessel were considered separately. This proved effective for the  $C_Y$  coefficient, but no consistent results were obtained for the  $C_X$  coefficient. For this reason, the longitudinal wind load determination is not as straightforward as the lateral wind load determination.

### Lateral Wind Force

From Equation 1

$$C_{YM} = \frac{F_Y}{\frac{1}{2} \rho V^2 A_Y} \quad (10)$$

Where  $C_{YM}$  is the experimentally measured value of the lateral wind drag coefficient at an incident wind angle of 90 degrees. By separating the total lateral force on a vessel into hull and superstructure components, a lateral drag coefficient ( $C_{YC}$ ) can be calculated. In this manner the general equation for  $F_Y$ , given by

$$F_Y = \frac{1}{2} \rho V^2 A_Y C_{YC} f(\theta) \quad (11)$$

can be written

$$F_Y = F_S + F_H = \frac{1}{2} \rho (\bar{V}_S^2 A_S + \bar{V}_H^2 A_H) C_{YC} f(\theta) \quad (12)$$

where subscripts S and H refer to the superstructure and hull, respectively, and  $\bar{V}$  denotes the mean wind velocity over each. Use of a constant drag coefficient ( $C_{YC}$ ) is considered valid because the hull and superstructure both appear as bluff bodies for lateral incident winds. Multiplying and dividing by the relative velocity ( $V_R$ ) at 33 feet gives:

$$F_Y = \frac{1}{2} \rho V_R^2 \left[ \left( \frac{\bar{V}_S}{V_R} \right)^2 A_S + \left( \frac{\bar{V}_H}{V_R} \right)^2 A_H \right] C_{YC} f(\theta) \quad (13)$$

From which

$$C_{YC} = F_Y / \left( \frac{1}{2} \rho v_R^2 \right) \left[ \left( \frac{\bar{v}_S}{v_R} \right)^2 A_S + \left( \frac{\bar{v}_H}{v_R} \right)^2 A_H \right] f(\theta) \quad (14)$$

where the values for  $(\bar{v}_H/v_R)^2$  and  $(\bar{v}_S/v_R)^2$  are taken from the wind gradient curve with  $n = 7$  (Figure 3), and are the values that correspond to the centers of area of the portions of the gradient curve that lie between the height ranges of the hull and superstructure of the ship. Values of  $C_{YC}$  for the experimental values presented in terms of Equation 10 were determined by taking the ratio of Equation 10 to Equation 14:

$$C_{YM} C_{YC} = \left[ \left( \frac{\bar{v}_S}{v_R} \right)^2 A_S + \left( \frac{\bar{v}_H}{v_R} \right)^2 A_H \right] / A_Y \quad (15)$$

Such that

$$C_{YC} = (C_{YM})(A_Y) \left[ \left( \frac{\bar{v}_S}{v_R} \right)^2 A_S + \left( \frac{\bar{v}_H}{v_R} \right)^2 A_H \right] \quad (16)$$

Representative  $C_{YC}$  values were determined using data from 17 of the 31 ship models, and estimated wind gradients from the tests when reported. Four of the  $C_{YC}$  values for these 17 representative ship models were discarded through comparisons to similar ship types and were attributed to questionable or incomplete data concerning the gradient or projected ship areas. A mean value was then determined from the remaining 13 models, yielding

$$C_{YC} = 0.92 \pm 0.1$$

This calculated value is consistent with an expected value of just less than 1, based on drag measurements of flat plates that yield coefficients of 1.1 to 1.2 (Ref 11), and the fact that the hull and superstructure are slightly streamlined in shape compared to a plate.

With the value of  $C_{YC}$  constant at 0.92, Equation 16 becomes

$$C_{YM} = 0.92 \left[ \left( \frac{\bar{V}_S}{V_R} \right)^2 A_S + \left( \frac{\bar{V}_H}{V_R} \right)^2 A_H \right] / A_Y \quad (17)$$

And using this peak coefficient value:

$$C_Y(\theta) = C_{YM} f(\theta) \quad (18)$$

### Lateral Wind Shape Function

The shape function,  $f(\theta)$ , versus incident angle was determined by transforming a normal sine wave into a more flat-topped sine wave, which was more characteristic of the lateral wind load coefficient plots for most of the 31 model ships analyzed. This transfigured shape function is a result of the summation of the standard sine wave with a sine wave of period 1/5 the size (Figure 15). The expression of this trial shape function ( $f'$ ) is

$$f'(\theta) = \sin \theta + M \sin 5\theta \quad \text{where } 0 \text{ degrees} \leq \theta \leq 180 \text{ degrees} \quad (19)$$

Substituting for  $\theta$ :

$$(A) \text{ at } \theta = 90 \text{ degrees, } f'(90) = 1 + M$$

$$(B) \text{ at } \theta = 72 \text{ degrees, } f'(72) = 0.95$$

Setting  $f'(90) = f'(72)$  to get the flat top, and solving for  $M$

$$0.95 = 1 + M; M = -0.05$$

Substituting this coefficient into the function,

$$f'(\theta) = \sin \theta - (\sin 5\theta)/20 \quad (20)$$

This trial shape function is now normalized as

$$f(\theta) = [\sin \theta - (\sin 5\theta)/20] / (1 - 1/20) \quad (21)$$

The final equation for the lateral wind drag force coefficient then becomes

$$C_Y(\theta) = C_{YM} \{[\sin \theta - (\sin 5\theta)/20] / (1 - 1/20)\} \quad (22)$$

Equation 21 gives the standard form for the shape function for both the lateral and longitudinal forces; changes in the constant (i.e., 20) and argument of the sine allow use of the same basic equation for a progression of shape functions.

### Longitudinal Wind Force

As previously stated, the separation method used for the lateral coefficient ( $C_Y$ ) was not successful for the longitudinal coefficient ( $C_X$ ) which assumed a hull coefficient of 0.4 based on the experimental data for hull dominated vessels. An alternative inspection method was used instead. The headwind coefficients of 19 of the model ships were analyzed, and it was found that ships with cluttered decks have headwind coefficients consistently higher than comparable ships with cleaner (trim) decks. Center island tankers were found to have headwind coefficients from 15% to 25% higher than single superstructure vessels, depending on trim or cluttered deck conditions.

The measured headwind coefficients of the 19 models were then adjusted, if necessary, according to the observations above, and a mean headwind coefficient of  $C_{XB} = 0.70 \pm 0.06$  was obtained, except for hull dominated ships (aircraft carriers) where the headwind coefficient obtained was  $C_{XB} \cong 0.40$ . The tailwind coefficients for these 19 ship models were also analyzed; it was found that: Single (simple) superstructure vessels generally have a tailwind coefficient  $C_{XS} \cong 0.60$ ; single superstructure cluttered (piping, masts, etc.) vessels and hull dominated vessels have  $C_{XS} \cong C_{XB}$ ; center island tankers have  $C_{XS} \cong 3/4 C_{XB}$ ; and distributed superstructure vessels (cruisers and destroyers) have  $C_{XS} \cong 1.1 C_{XB}$ .

The longitudinal wind load coefficient shape function has positive and negative portions that require a separate curve fit for each. The zero crossing point,  $\theta_z$ , must be known in order to join these two curves. The major factor, which determines the value of  $\theta_z$ , was found to be superstructure location. For hull dominated ships it was found that  $\theta_z \cong 120$  degrees. For single superstructure ships with clean decks, the value of  $\theta_z$  varied by a full 20 degrees depending upon superstructure location;  $\theta_z \cong 80$  degrees for a superstructure centered forward of the centerline,  $\theta \cong 90$  degrees for a superstructure close to the centerline, and  $\theta \cong 100$  degrees for an aft superstructure. A value  $\theta \sim 100$  degrees is recommended as a representative value for most ships.

Looking at the longitudinal shape functions for all 31 of the ship models, two major types were found; a cosine wave and a "humped" cosine wave. The cosine wave is characteristic of the single superstructure ships with trim decks and hull dominated vessels, while the "humped" cosine wave is more characteristic of all other ship types analyzed. For simplicity, the same shape function used for the lateral loads was used for the longitudinal loads. The value  $M = 1/20$  was changed to  $M = 1/10$  for the  $C_X$  coefficient (Figure 6) and the shape function for  $C_X$  then becomes

$$f(\theta) = \left( \sin \psi - \frac{\sin 5\psi}{10} \right) / (1 - 1/10) \quad (23)$$

where  $\psi$  depends on  $\theta$  and  $\theta_z$ . This is essentially the same as Equation 21. Now, determining  $\psi$  for the positive portion of the curve fit using

$$\psi = M \theta + b \quad (24)$$

results in

$$\psi^{(+)} = \left( \frac{90}{\theta_z} \right) \theta + 90 \quad (\theta < \theta_z) \quad (25)$$

For the negative portion of the curve, using the same procedure,

$$\psi^{(-)} = \left( \frac{90}{180 - \theta_z} \right) \theta + \left( 180 - \frac{90 \theta_z}{180 - \theta_z} \right) \quad (\theta > \theta_z) \quad (26)$$

so that

$$C_X^{(+)} = C_{XB} f \psi^{(+)} \quad \psi^{(+)} \text{ from Equation 25, } (\theta < \theta_Z) \quad (27)$$

$$C_X^{(-)} = C_{XS} f \psi^{(-)} \quad \psi^{(-)} \text{ from Equation 26, } (\theta > \theta_Z) \quad (28)$$

These apply only to humped cosine curve types, while the shape functions for the straight cosine curve shape are simply

$$f(\psi) = \cos \psi \quad (29)$$

$$\psi^{(+)} = \left( \frac{90}{\theta_Z} \right) \theta \quad (\theta < \theta_Z) \quad (30)$$

$$\psi^{(-)} = \left( \frac{90}{180 - \theta_Z} \right) (\theta - \theta_Z) + 90 \quad (\theta > \theta_Z) \quad (31)$$

#### Wind Yaw Moment

The yaw moment response ( $C_N$ ) is more difficult to predict than the  $C_X$  and  $C_Y$  responses because of the difficulties of accurately determining the moment arms and interference effects of the superstructure and other topside features that significantly add to the wind drag on each ship, and because of a pronounced sensitivity to freeboard in many ships. Hence, no curve fit was attempted, and all findings are based entirely upon the observed moment coefficient curve of each model. Generalizations concerning the moment response with respect to superstructure location and apparent trends for the ship types covered are presented below.

The location of the superstructure seems to be the best indicator of a ship's moment response. According to the conventions of this report, as the main superstructure of a vessel progresses from stern to bow, the moment tends from a positive to a negative orientation, as shown in Figure 7. Similar to the definition of the  $C_X$  coefficient, the value of  $\theta_Z$  is the incident wind angle at which the  $C_N$  coefficient crosses the

axis, changing from a negative to a positive moment (by the conventions established in this report). Based on the experimental data used, the following values of  $\theta_z$  and magnitude ratios of negative to positive moment are given for the yaw moment coefficient curves of the model ship types analyzed.

1. Single superstructure ships, grouped by location:

a. Stern

Trim -  $\theta_z \cong 60$  degrees; 1:3  
Cluttered -  $\theta_z \cong 80$  degrees; 1:2

b. Between stern and center

$\theta_z \cong 80$  degrees; 1:3

c. Center

$\theta_z \cong 90$  degrees; 1:1

d. Between center and bow

$\theta_z \cong 105$  degrees; 1:1

2. Center Island Tankers:

Trim -  $\theta_z \cong 85$  degrees; 1:2  
Cluttered -  $\theta_z \cong 85$  degrees - 90 degrees; 1:1

3. Distributed superstructure ships:

Cruisers

$\theta_z \cong 90$  degrees - 100 degrees; 1:1

Destroyers

$\theta_z \cong 110$  degrees; 4:1

4. Hull dominated ships:

Aircraft carriers

$\theta_z \cong 90$  degrees - 100 degrees; 1:1

Passenger liners

$\theta_z \cong 100$  degrees; 2:1

Although useful, the above information is limited because the magnitude ratios are strictly relative, with no reference coefficient values given. The magnitude of the moment coefficient curve is dependent

on the size of projected superstructure and hull areas and the moment arms through which they act. Therefore, since no approximation for the actual magnitudes of the moment coefficient is given, example moment curves have been provided for all ship types dealt with in this analysis. These curves are presented in Figures 8 through 14, representing the best estimates (averages) attainable from the experimental model data used.

#### ATYPICAL SHIP TYPES

The methods presented in this report for calculating wind drag coefficient curves are primarily geared toward tankers and cargo ships, since these comprised the majority of the ship models investigated. Even so, these same methods proved adequate for the warships that were present in the experimental model data used. There are, however, several uncharacteristic design features which create atypical ship types not entirely compatible with the suggested methods of this report. One such atypical ship is the Kumo, which possesses an aft superstructure somewhat larger than normal with respect to the overall length of the ship and an extremely prominent forecastle. Collectively, these two uncharacteristic features cause a considerable increase in the headwind coefficient ( $C_{XB}$ ) for the  $C_X$  wind load response to a value near 1.0, and an increase in the peak  $C_Y$  coefficient to a value between 0.90 - 1.0 in magnitude. The moment response ( $C_N$ ) is essentially unaffected, with  $\theta_z \cong 60$  degrees and a magnitude ratio of 1:3 for the negative to positive moment orientation.

Other atypical ship types, at least for the purposes of this report, are the smaller auxiliary and research vessels such as the METEOR. These vessels have a distributed upper deck layout that causes them to behave very much like a destroyer in their wind load responses.

All other atypical ships (submarines, catamarans, hydrofoils, etc.) were not investigated in this study, so the use of the design methods presented in this report for determining the loads on such ships is not recommended.

## DISCUSSION OF RECOMMENDED PROCEDURES

To provide the reader with a better perspective regarding the accuracy and practicality of the methods recommended here, comparisons will be made to representative experimental results and recommendations from earlier investigators.

### Comparisons to Experimental Data

Figures 16 through 19 illustrate longitudinal coefficients ( $C_X$ ) for most ships and allow for an evaluation of the design procedures recommended here. Figure 16 shows  $C_X$  values for the simplest type of ships; the recommendations for  $C_{XB} = 0.70$ , a cosine shape function, and variable zero crossing values are reasonable for this application. Figure 17 shows  $C_X$  values for center island tankers; the recommendations of  $C_{XB} \cong 0.8$  or  $C_{XB} \cong 0.9$ , a humped cosine shape function, and  $\theta_z \sim 100$  degrees are demonstrated. Similarly, Figure 18 shows  $C_X$  values for ships with distributed superstructures; note that  $C_{XS}$  values are larger than  $C_{XB}$  values, as noted in the SUMMARY OF WIND FORCE EQUATIONS section. Finally, Figure 19 shows hull dominated vessels; note the extreme  $\theta_z \sim 120$  degree value, and the extreme behavior of the "Fahrgastshiff" (see Figure 2 for silhouette). Otherwise, the results are nearly identical.

Figures 20 through 22 show representative lateral coefficients ( $C_Y$ ). However, only a discussion on the shape function is applicable here, since the design methods presented in this report allow for variable values of the peak coefficient.

Figure 20 shows the "usual" sinusoidal shape function used by most designers. As shown, this shape function certainly applies to these vessels. However, Figure 21 shows the type of behavior recommended in this report as typical for most ships. The flattened behavior of these responses are evident; in fact, more vessels fell into this category than the former. Figure 22 shows an even more extreme type of behavior measured for some ships, which seems to suggest a "double-humped" behavior.

With all three of these figures, no clear indications as to vessel types versus shape category types were discovered, and the middle-of-the-road shape of Figure 21 was used as generally applicable to all ships. It is evident now why the general form of the shape function was retained in Equations 3 and 6; it allows the user to easily tailor the characteristic shape of the load versus angle to whatever is considered best.

The question of error in the yaw moment coefficients is also applicable to all the specialized coefficients presented in Figures 8 through 14 in this report. Care was taken to collect as much data as possible for each ship type before deciding on a "recommended" curve, which resulted in consistent and recognizable trends for the ship types used here. Defining the error associated with each recommended curve is difficult; however, Figure 23 illustrates a typical ship-type comparison for center island tankers. It is seen that the use of an average value in this case is entirely justified as representative of most center island tankers.

It should be pointed out that the yaw moment can be very sensitive to vessel draft; the yaw moment response of a supertanker can approximate the response given in Figure 8 if it is unloaded (and therefore hull dominated), but change to Figure 9 when loaded (and therefore stern island dominated). This behavior is not characteristic of ships with a centered superstructure arrangement, but some caution should be used in applying these recommended moments.

#### Comparison to Other Investigators

The peak lateral coefficient value of  $C_y = 0.92 \pm 0.1$  compares favorably to the value of  $C_y = 0.871$  with a 23% deviation as calculated by Altmann (Ref 12) from the test data of Reference 5. The longitudinal coefficient value of  $C_x = 0.70 \pm 0.06$  is more accurate than Altmann's value of  $C_x = 0.796 \pm 0.19$  for normal ships. The agreement is closer for the hull dominated ships with  $C_x \cong 0.40$  compared to Altmann's  $C_x = 0.363$ . These latter values for hull dominated vessels are higher than those given by Hughes (Ref 7), where only one-third of the total hull area (thus  $C_x = 0.33$ ) was used in calculating the wind load forces.

Figure 24 is Figure 7 replotted with recommended yaw moment coefficients from References 1 and 12. This illustrates the possible errors associated with the use of any single moment curve, regardless of the source.

#### CONCLUSIONS AND RECOMMENDATIONS

The primary goals of this investigation have been achieved in that the methods for calculating wind drag loads on many types of ships can now be carried out in a simple yet individualized manner. Although the proposed approach is less complex than that of others, its value is readily evident from a practical standpoint.

It is recommended that the methods presented in this report be used primarily for the determination of wind drag loads on tankers and cargo ships; they can also be applied to other conventional ship types (including warships) with a reasonable degree of confidence.

Finally, several other sources used in the preparation of this paper, not directly referenced in the text, are listed in References 13 through 17. An example of a typical wind load and moment response determination is presented in the Appendix.

#### ACKNOWLEDGMENT

Sincere thanks go to Miss Patricia Alvarado, who transposed the data from the various experimental reports into the coordinate system used in this study and who attempted the first coefficient comparisons.

#### REFERENCES

1. Naval Facilities Engineering Command. Design Manual 26.6: Mooring design physical and experimental data, Alexandria, Va., 1980, (Preliminary Draft)

2. P. A. Palo and R. L. Webster. "Static and dynamic moored tanker response," in Computational Methods for Offshore Structures, edited by H. Armen and S. Stiansen. New York, American Society of Mechanical Engineers, 1980, pp. 135-146 (AMD, vol 37).
3. V. B. Wagner. "Windkräfte and Überwasserschiffen," Schiff Und Hafen, Hamburg, 1967.
4. Naval Facilities Engineering Command. Design Manual DM-26: Harbors and coastal facilities, Alexandria, Va., 1968.
5. K. D. A. Shearer and W. M. Lynn. "Wind tunnel tests on models of merchant ships," International Shipbuilding Progress, vol 8, no. 78, Feb 1961, pp. 62-80.
6. G. R. Mutimer. Wind tunnel tests to determine aerodynamic forces and moments on ships at zero heel, David Taylor Naval Ship Research and Development Center, Report 956, Aero Data Report 27, Mar 1955.
7. G. Hughes. "Model experiments on the wind resistance of ships," Institution of Naval Architects, Transactions, vol 72, 1930, pp. 310-325; discussion, pp. 326-330.
8. R. W. F. Gould. Measurements of the wind forces on a series of models of merchant ships, National Physical Laboratory, Aerodynamics Division, Teddington, U. K., Aero Report 1233, Apr 1967.
9. J. J. Myers, et al, eds. Handbook of ocean and underwater engineering. New York, McGraw-Hill, 1969.
10. Columbia University, Hudson Laboratories. Report No. ARTEMIS-65-Vol. 1: A dynamic position keeping system installed aboard the USNS Mission Capistrano (TAG - 162), vol 1. Preliminary design considerations and installation, by H. C. Beck and J. O. Ess. Dobbs Ferry, N.Y., Aug 1968. (AD 860 376L)

11. S. F. Hoerner. Fluid-dynamic drag. Midland Park, New Jersey, 1965.
12. R. Altmann. Forces on ships moored in protected waters, Hydronautics, Inc., Technical Report 7096-1, 1971, Laurel, MD.
13. G. F. M. Remery and G. von Oortmerssen. "The mean wave, wind and current forces on offshore structures and their role in the design of mooring systems," in Preprints, 5th annual Offshore Technology Conference, vol 1, pp. 169-184, Dallas, Texas, 1973. (OTC 1741)
14. R. M. Isherwood. "Wind resistance of merchant ships," Royal Institution of Naval Architects, Supplementary Papers, vol 115, Nov 1973, pp. 327-338.
15. British Ship Research Association. Report NS. 256: Research investigation for the improvement of ship mooring methods; prepared by Chamber of Shipping of the United Kingdom. Wallsend, Northcumberland, England, 1969.
16. David W. Taylor Naval Ship Research and Development Center. Report SPD-716-01: A survey of wind loads on ocean facility structures, by N. T. Tsai. Bethesda, MD, Aug 1977. (AD A047800)
17. Oil Companies International Marine Forum. Prediction of wind and current loads on VLCC's, London, 1977.

## NOMENCLATURE

$A_H$	Lateral projected area of the hull only
$A_S$	Lateral projected area of the superstructure only
$A_X$	Longitudinal projected area of the ship
$A_Y$	Lateral projected area of the ship
$C_N$	Nondimensional yaw moment coefficient
$C_X$	Nondimensional longitudinal wind force coefficient
$C_{XB}$	Longitudinal headwind (bow) coefficient [ $C_X$ at $\theta = 0$ degrees]
$C_{XS}$	Longitudinal tailwind (stern) coefficient [ $C_X$ at $\theta = 180$ degrees]
$C_Y$	Nondimensional lateral wind force coefficient
$C_{YC}$	Calculated peak lateral force coefficient; constant = $0.92 \pm 0.1$
$C_{YM}$	Measured peak lateral force coefficient (from data)
$f(\theta)$	Normalized shape functions
$F_X$	Longitudinal wind force
$F_Y$	Lateral wind force
$N$	Yaw moment
$V$	Wind velocity
$V_R$	Reference wind velocity at 33 feet above sea

- $(\bar{V}_H/V_R)$  Average normalized wind velocity over hull
- $(\bar{V}_S/V_R)$  Average normalized wind velocity over superstructure
- $\theta$  Incident wind angle with respect to the ship
- $\theta_z$  Zero crossing angle
- $\rho$  Density of air

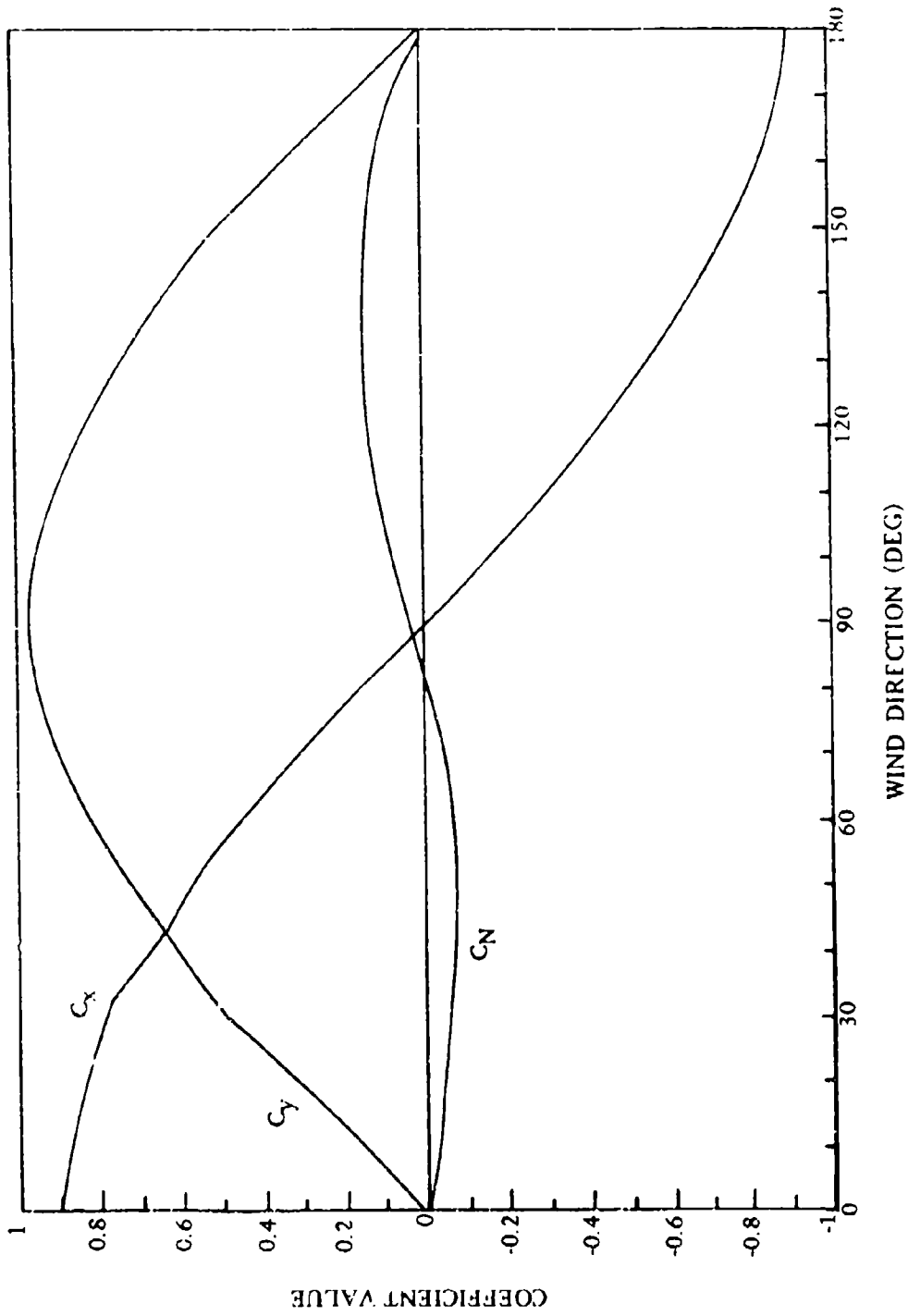


Figure 1. Suggested wind load coefficients from Reference 1.

Naval Vessels



Large Carrier (CVA-59)



Escort Carrier (CVE-55)



Heavy Cruiser (CA-139)



Light Cruiser (CL-145)



Destroyer (DD-692)



Amphibious Transport (APA-248)



Liberty Ship (LC-2)



T-AO Navy Tanker (AO-143)

Vessels Used in Figure 6



Cargo A



Cargo B (aft)



Cargo C (frd)



Seeschlepper

Miscellaneous Representative Vessels



Kuno



Fahrgastschiff



Hecktrawler



Meteor



Tanker A



Cargo C

Figure 2. Representative vessel profiles taken from the total listing in Table 1.

Variable Wind Gradients  
(N = 5, 7, 10)

Height Above Sea (ft)

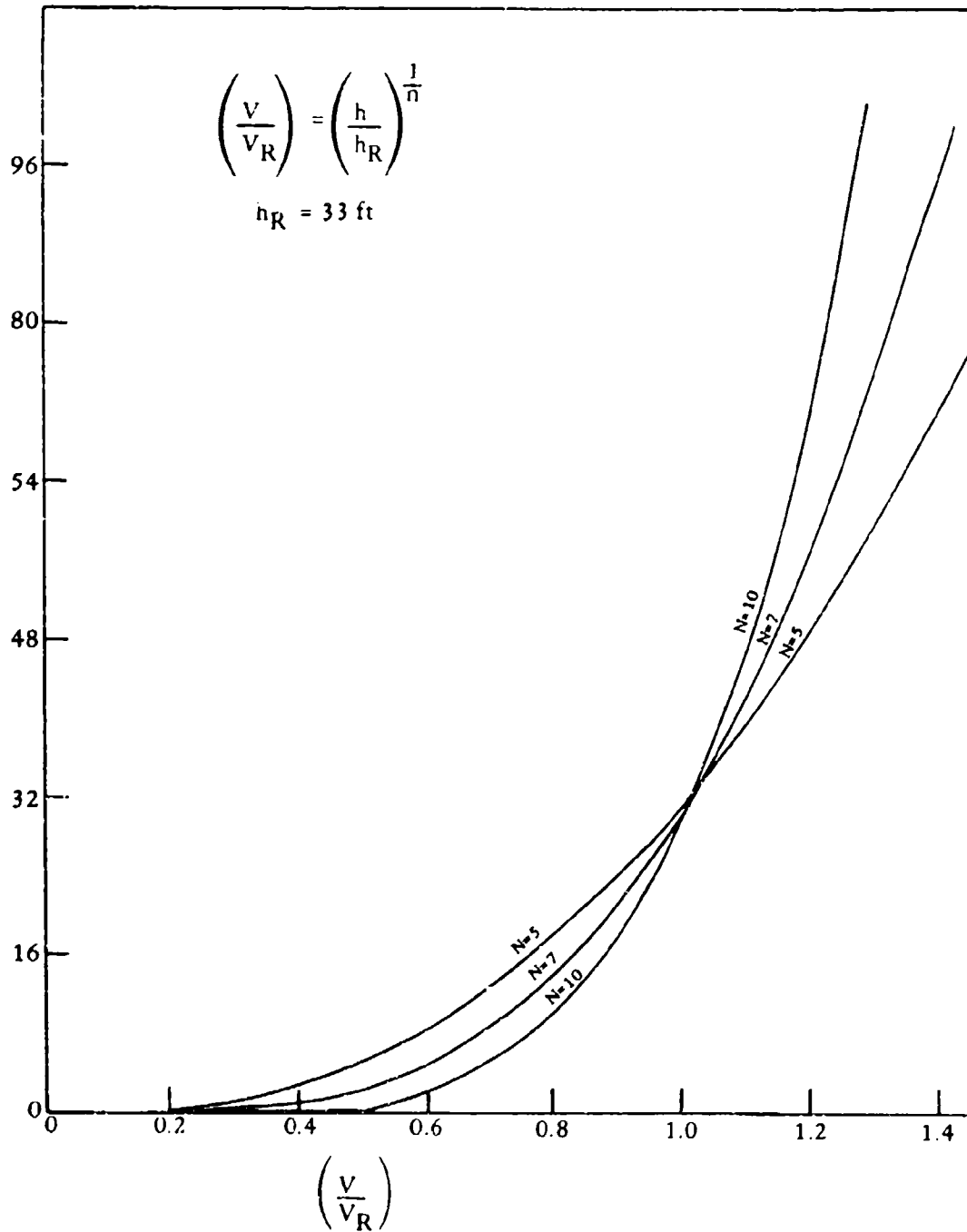


Figure 3. Wind gradient family.

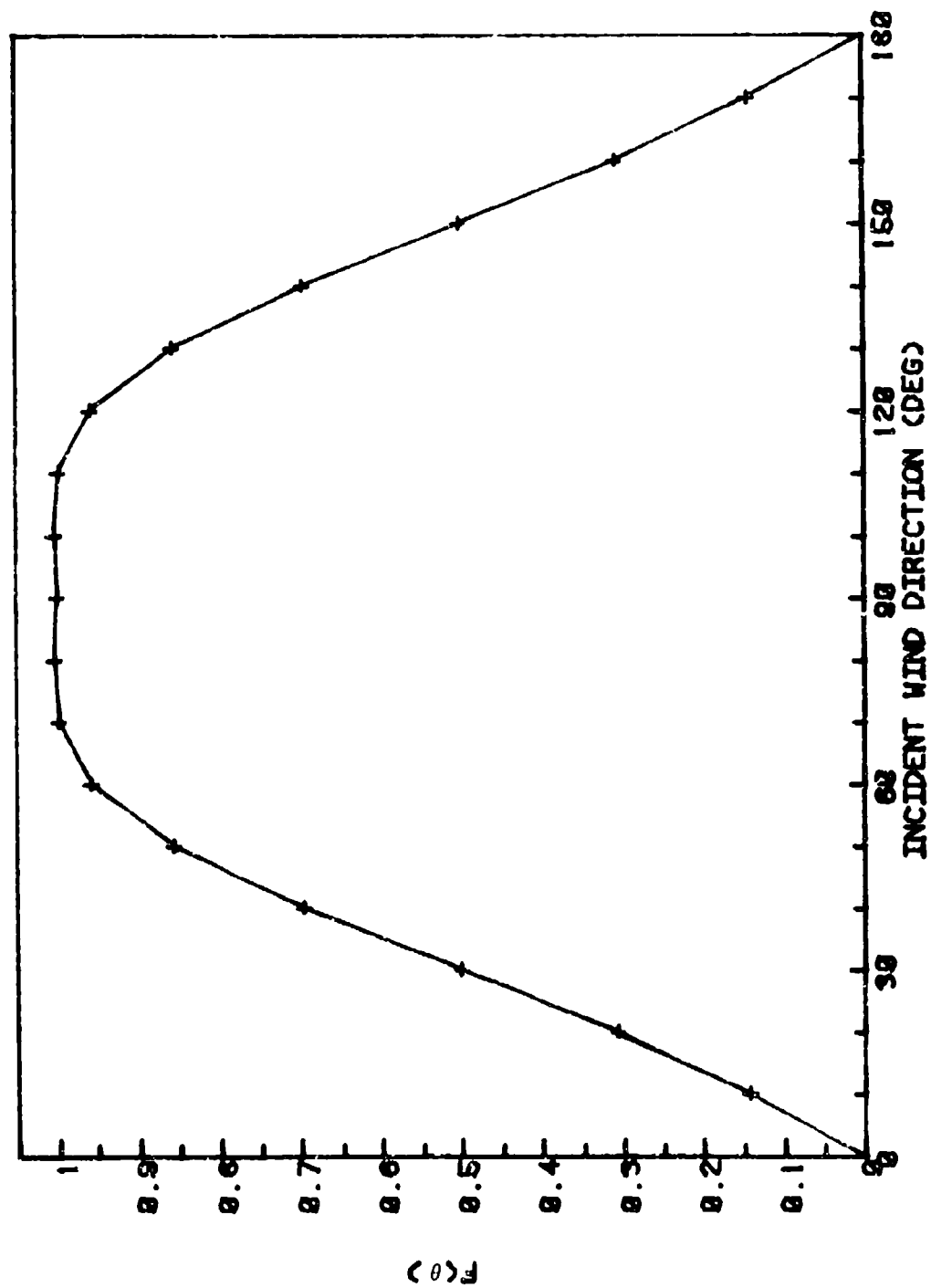


Figure 4. Lateral wind load shape function.

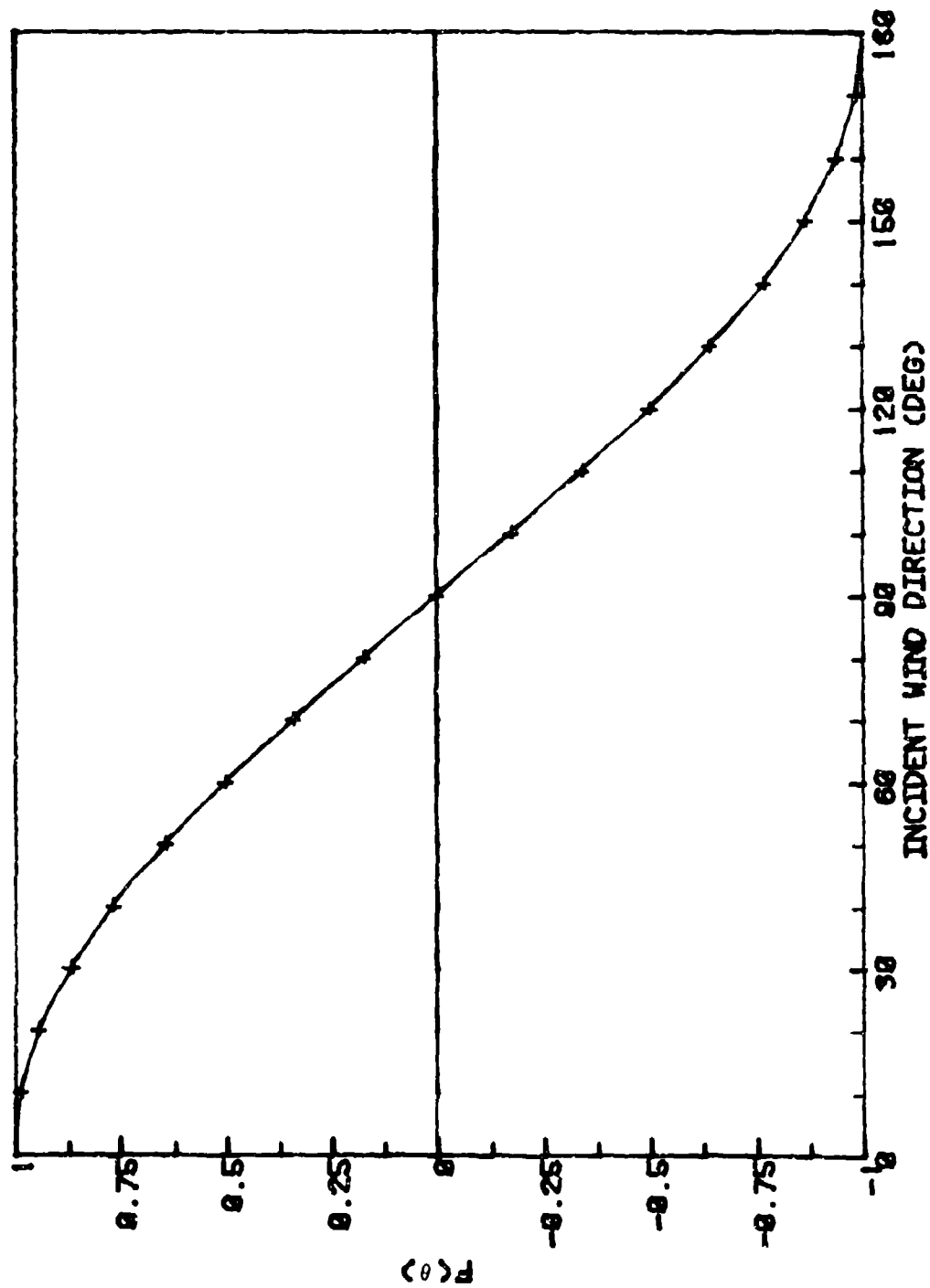


Figure 5. Longitudinal wind load shape function.

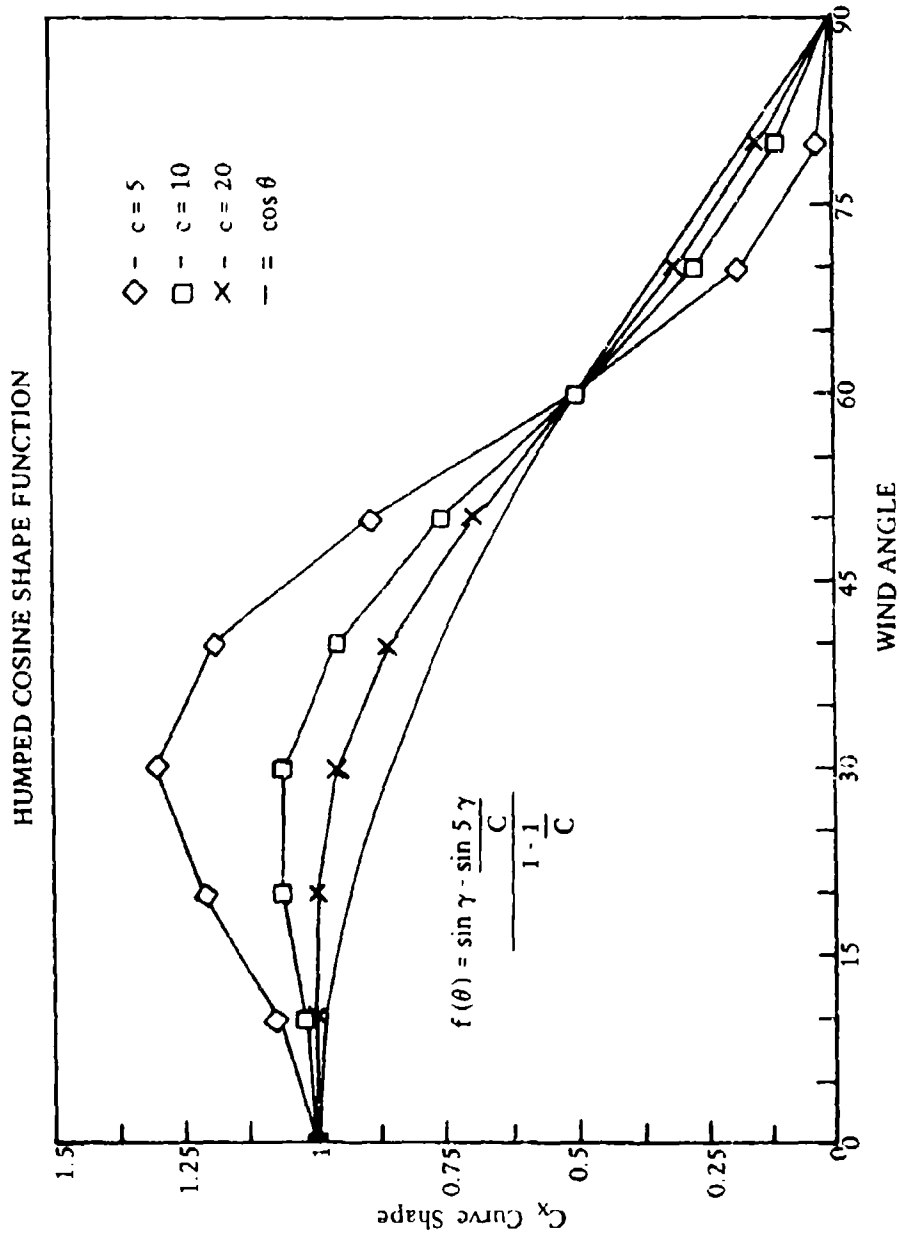


Figure 6. Family of curves for the longitudinal shape function.

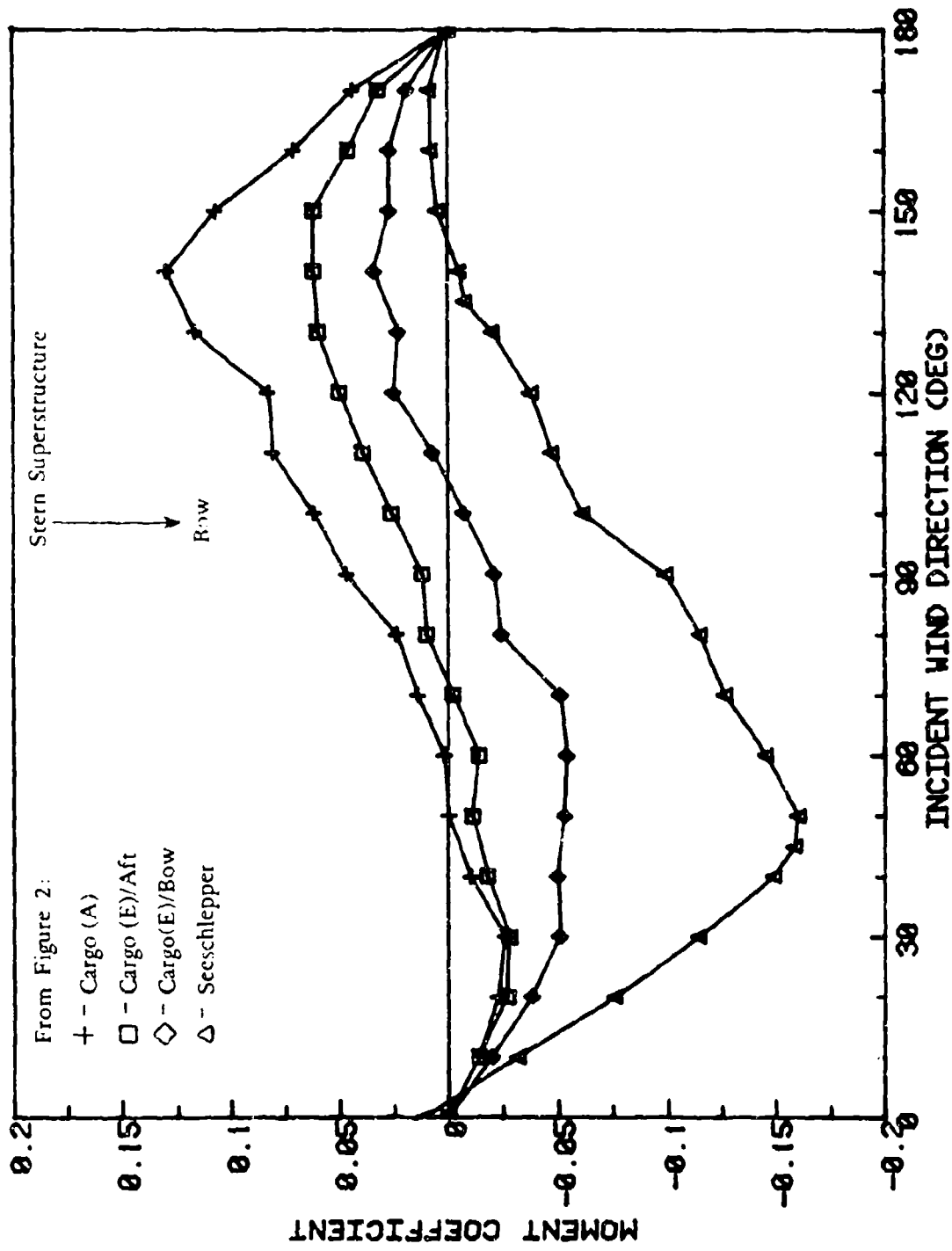


Figure 7. Wind yaw moment versus superstructure location.

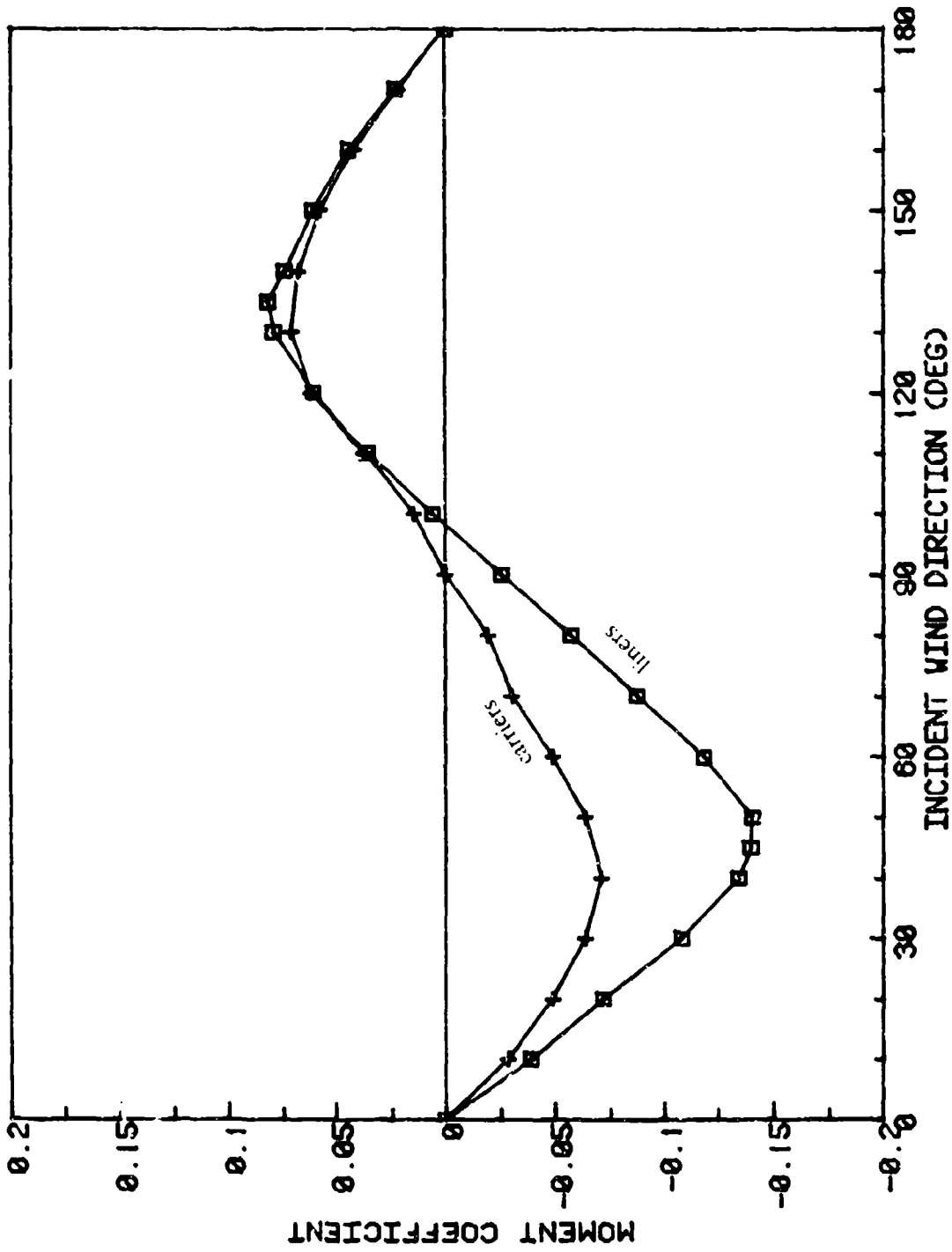


Figure 8 Recommended yaw moment coefficients for hull dominated vessels.

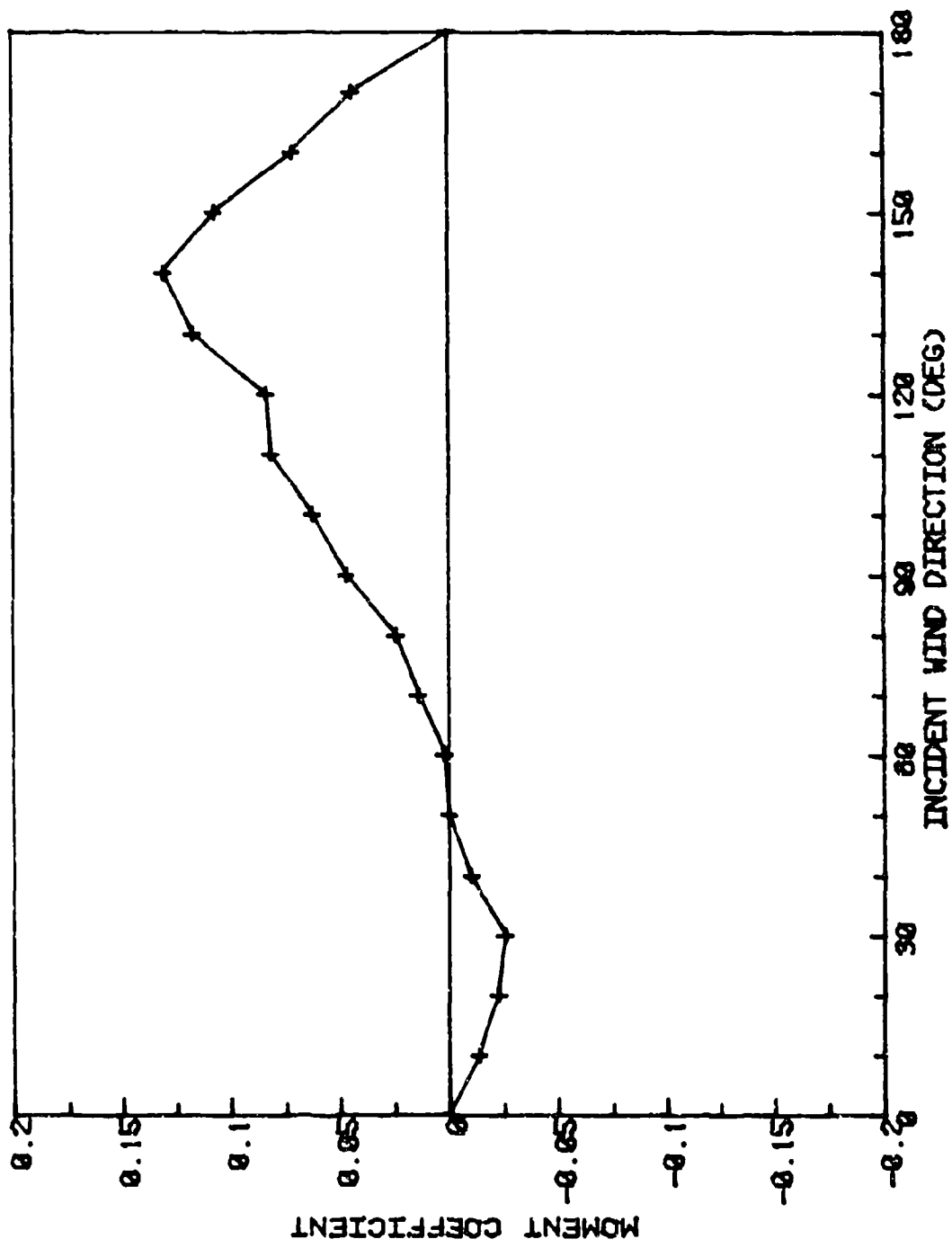


Figure 9. Recommended yaw moment coefficient for Stern Island vessels.

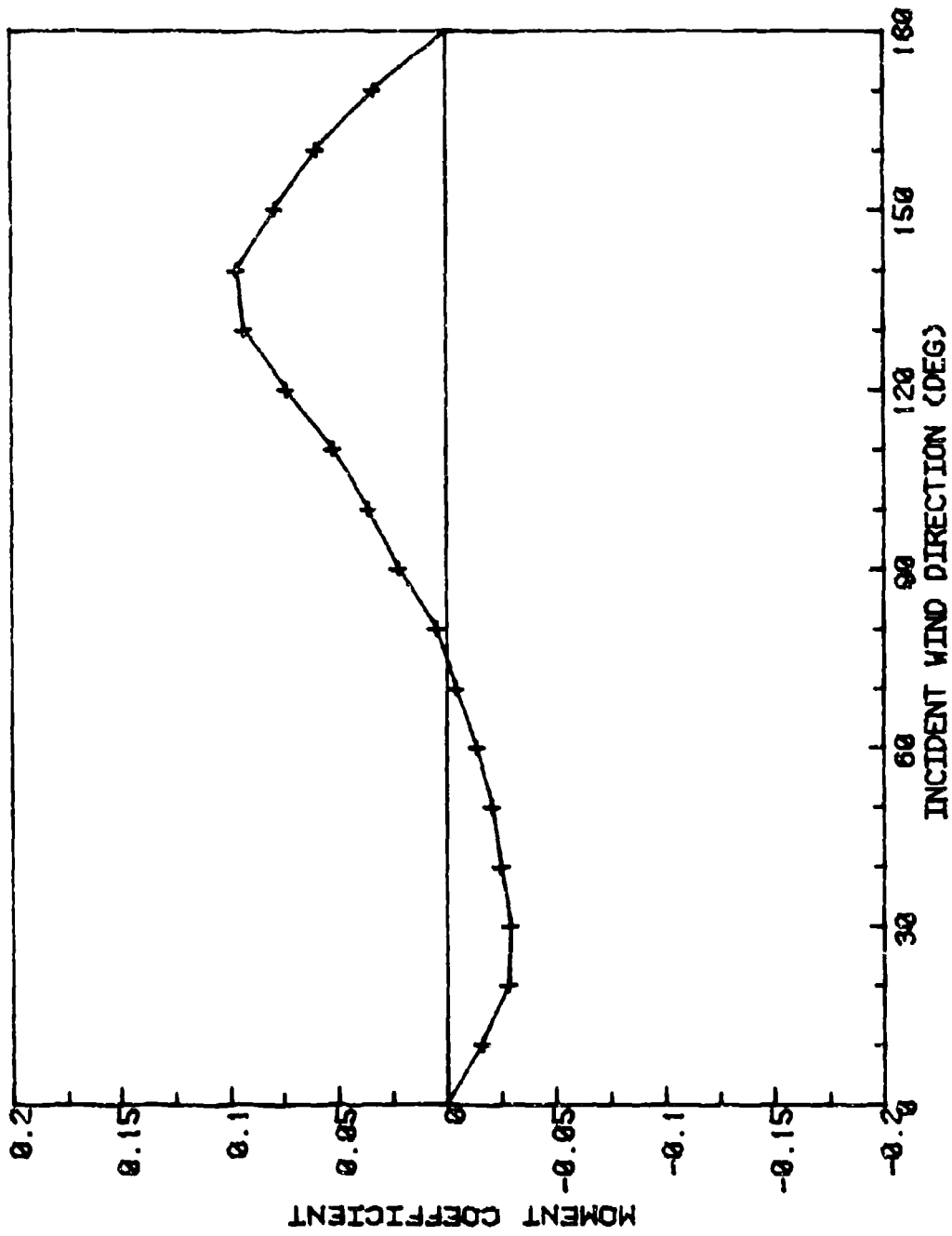


Figure 10. Recommended yaw moment coefficient for vessels with superstructure just aft of midship.

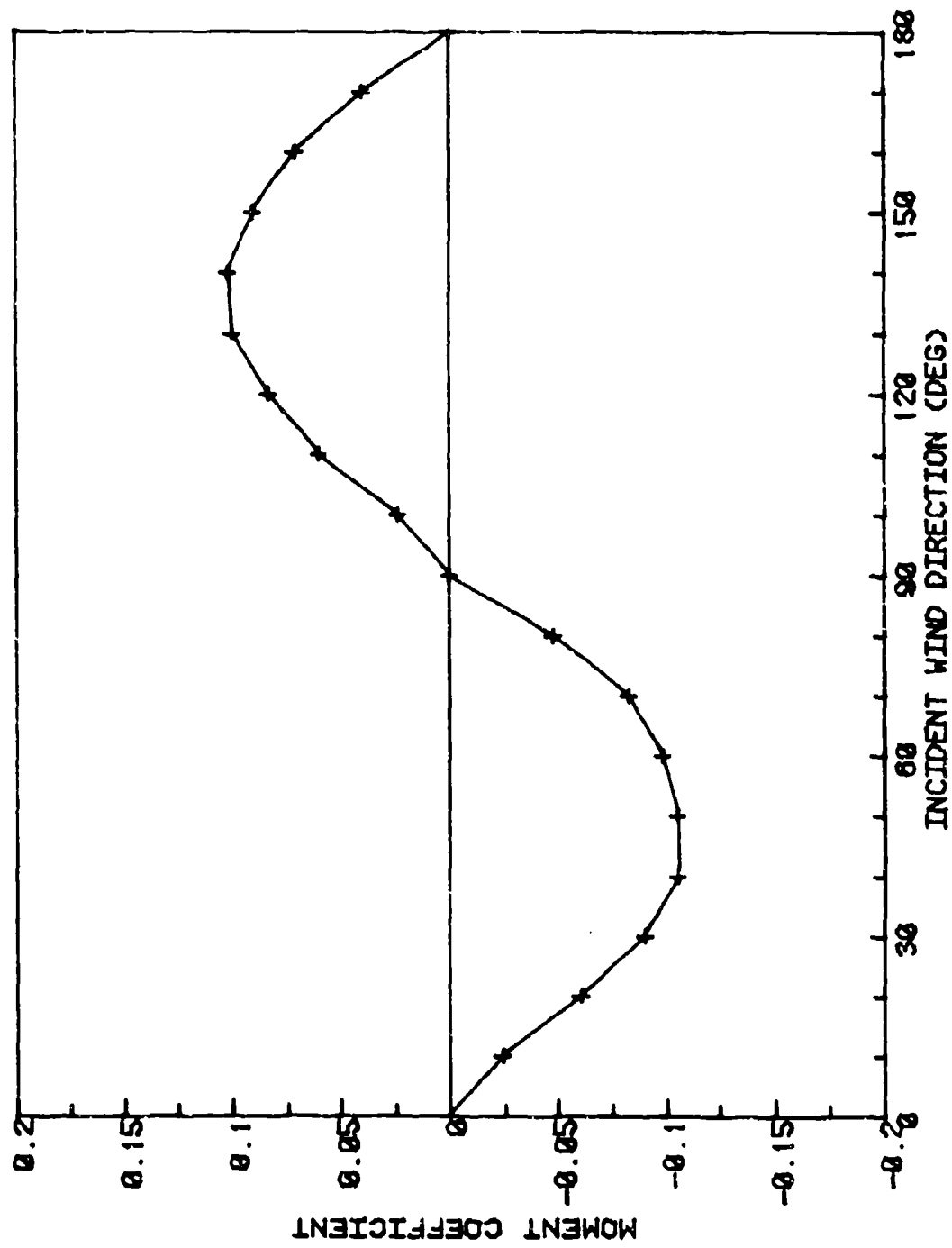


Figure 11. Recommended yaw moment coefficient for centered superstructure vessels.

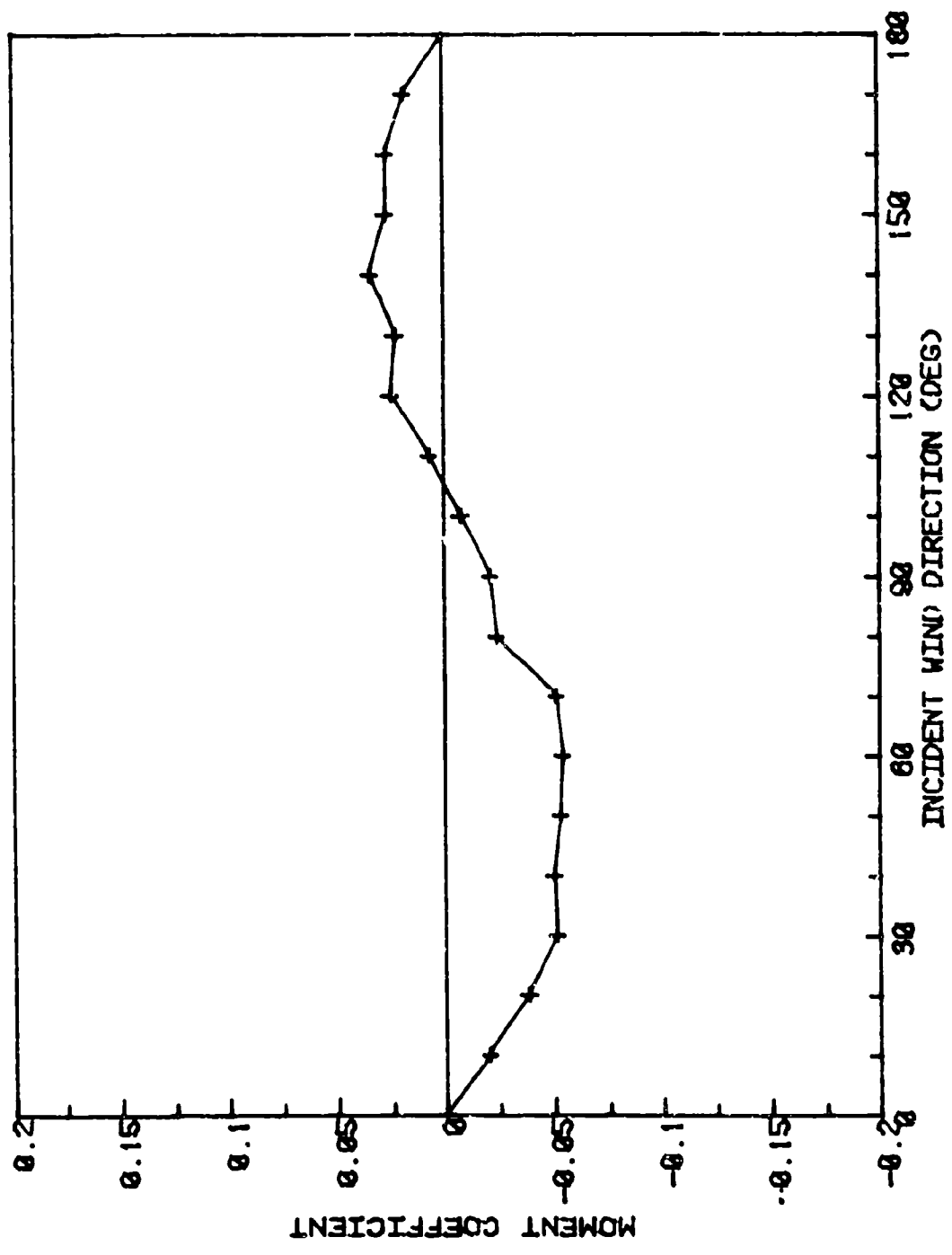


Figure 12. Recommended yaw moment coefficient for vessels with superstructure forward of the midship.

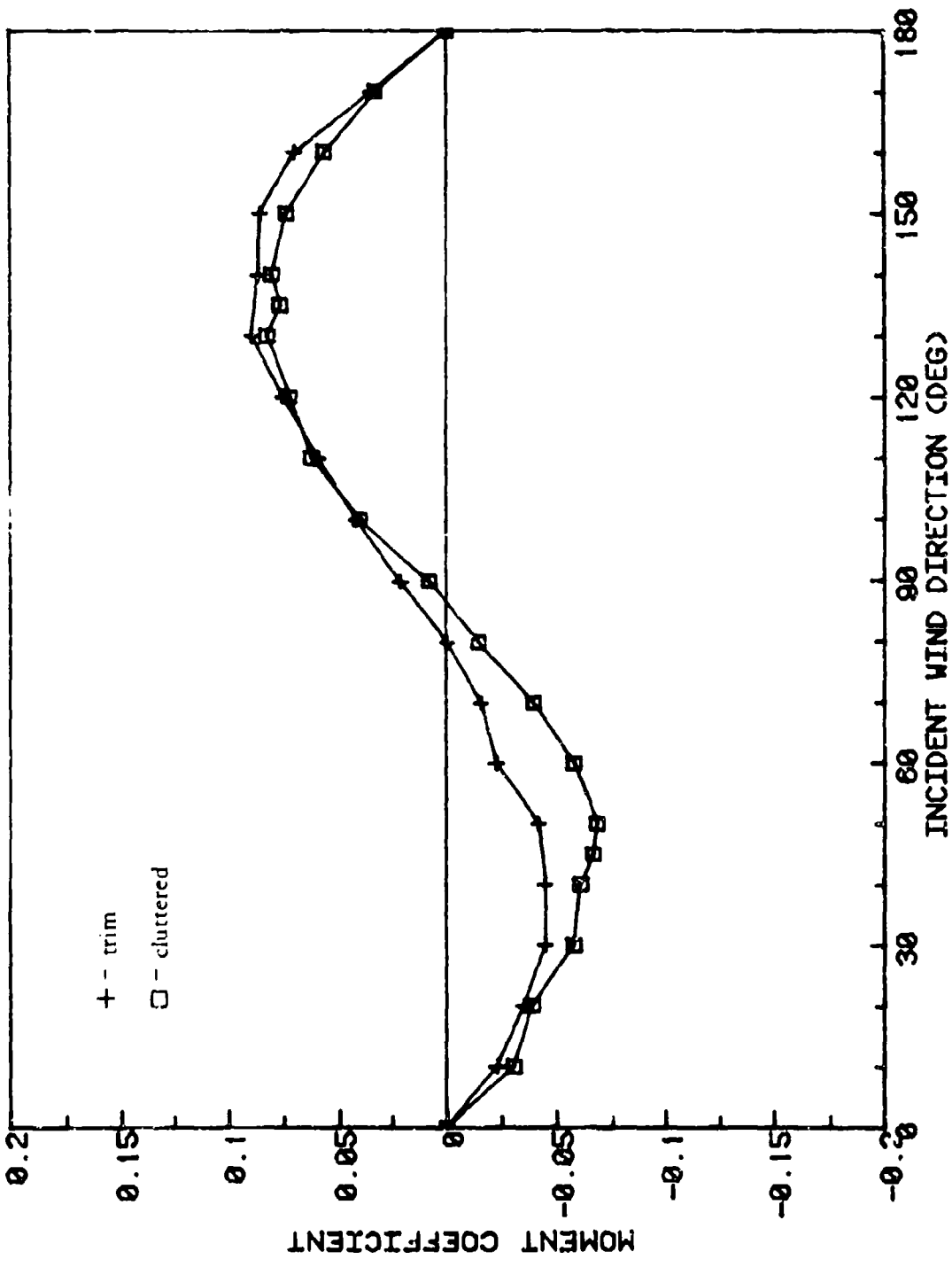


Figure 13. Recommended yaw moment coefficients for center-bladed tankers

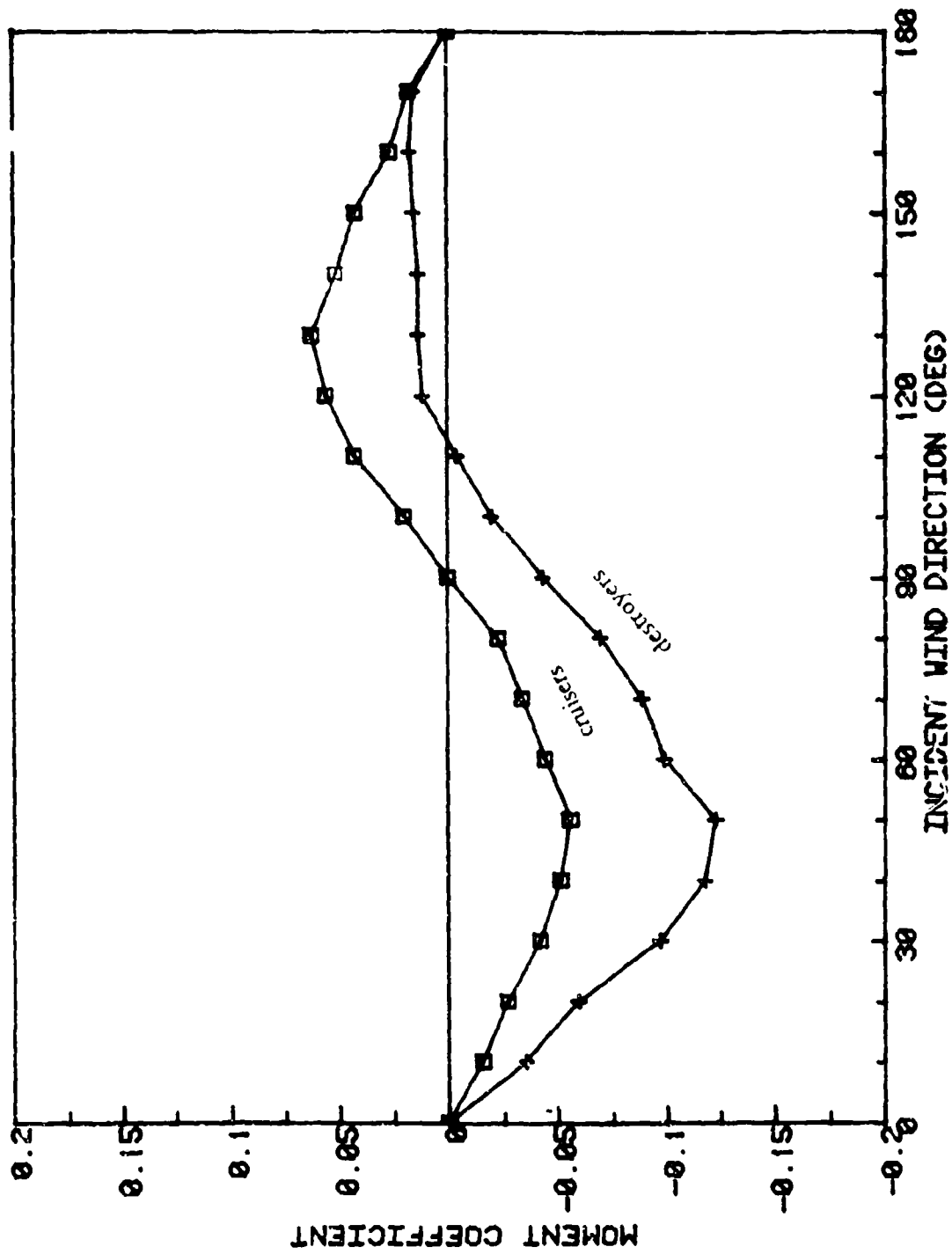


Figure 14. Recommended yaw moment coefficients for typical Naval warships.

General Curve Shape  
Adaptation

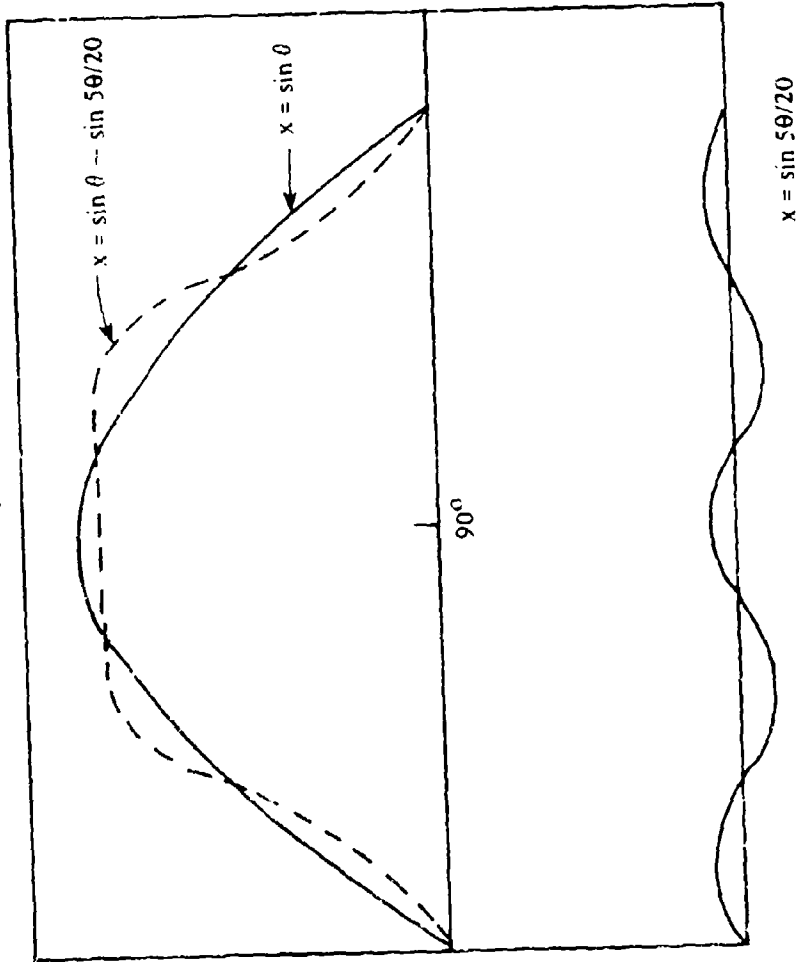


Figure 15. Lateral shape function components.

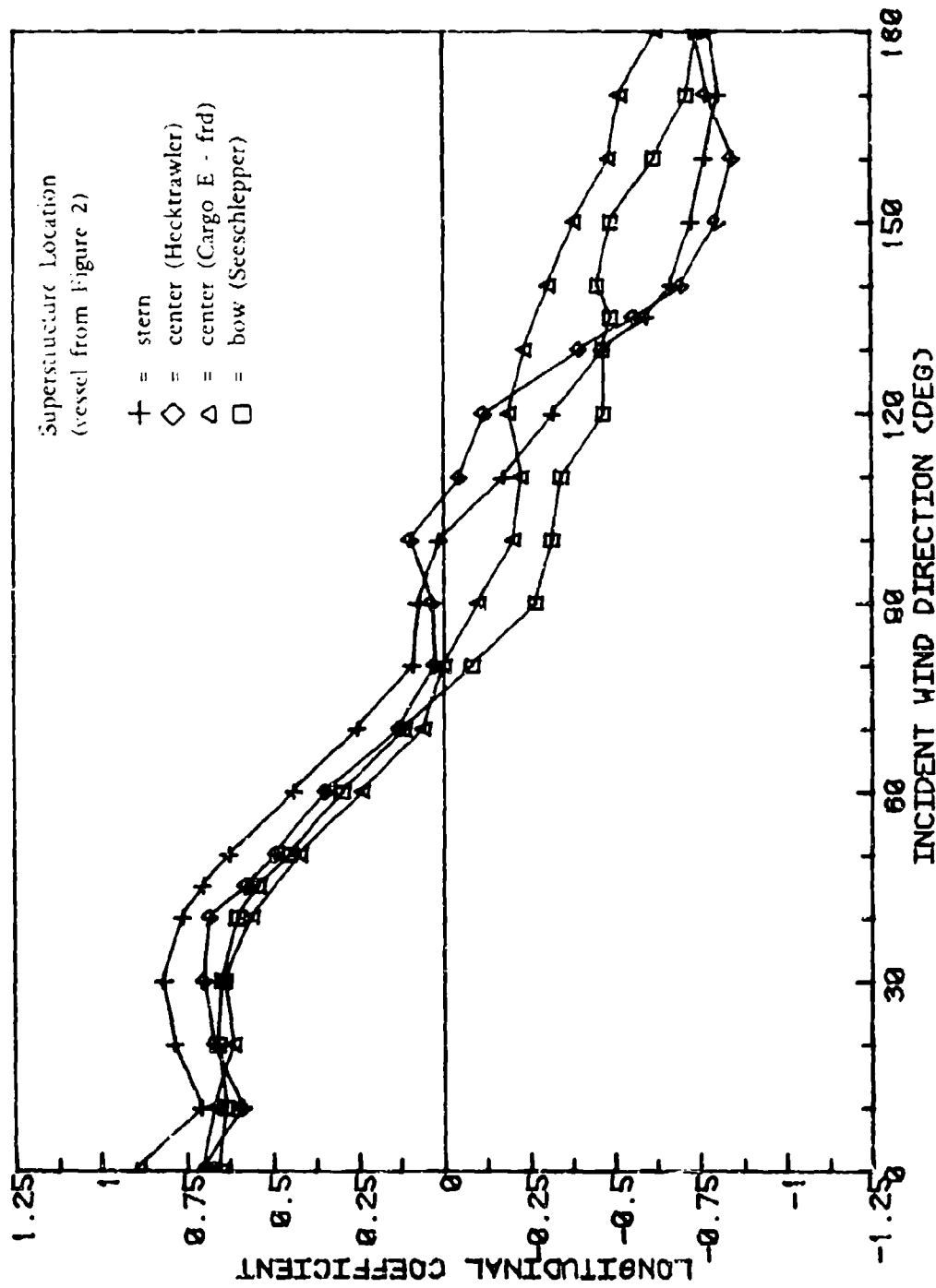


Figure 16. Representative longitudinal coefficients for single superstructure vessels

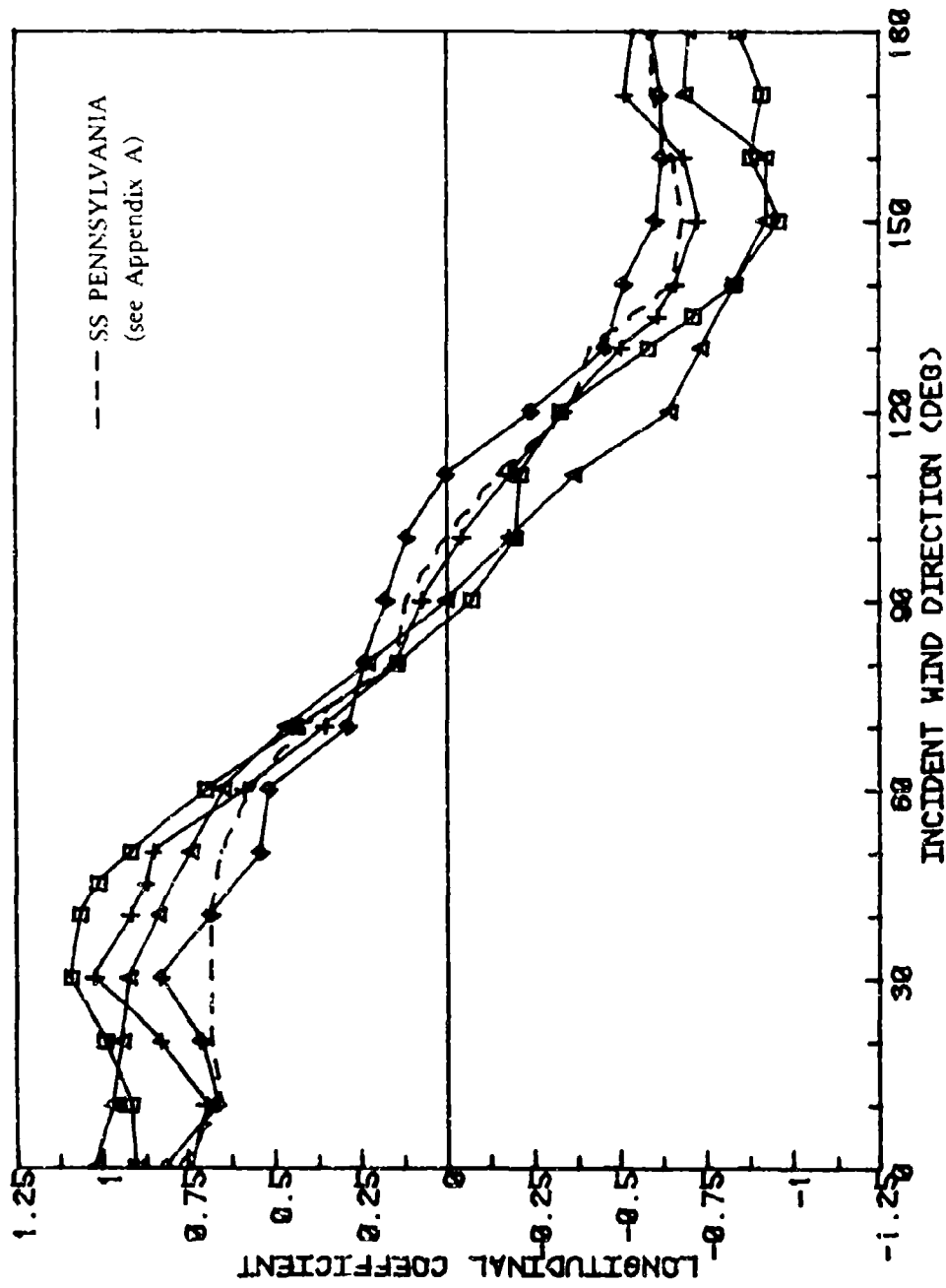


Figure 17. Representative longitudinal coefficients for center island tankers.

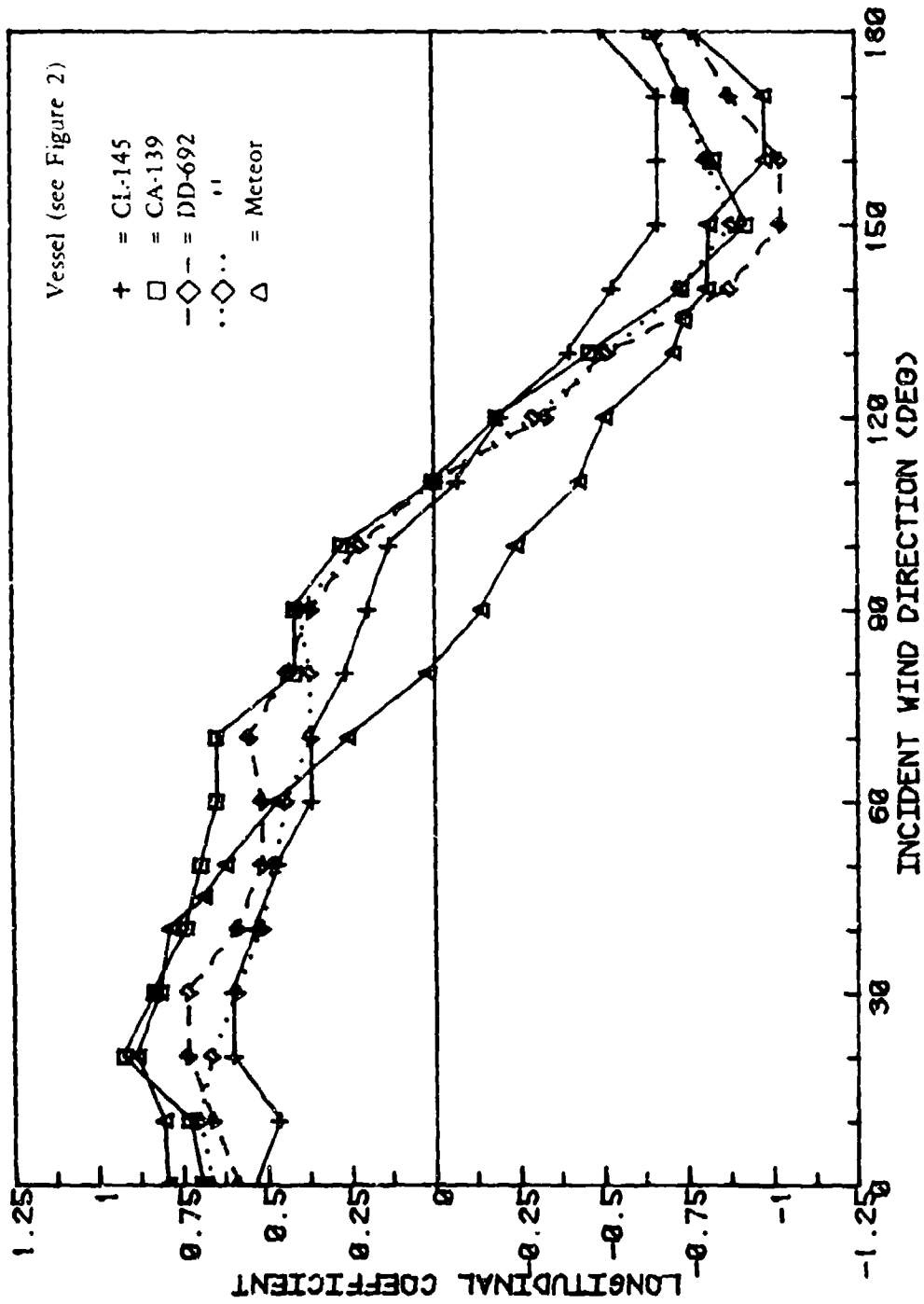


Figure 18. Representative longitudinal coefficients for vessels with distributed superstructures.

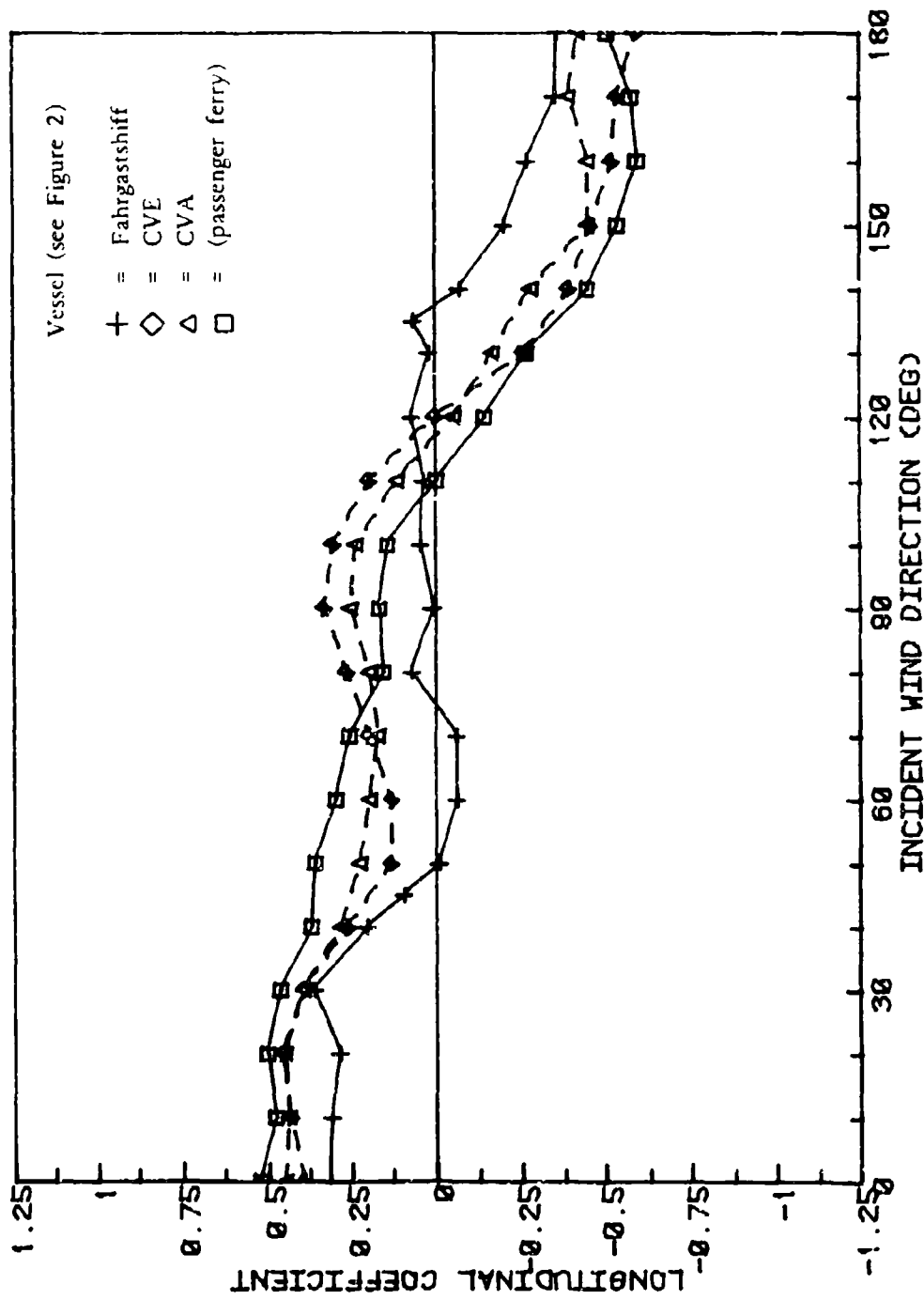


Figure 19. Representative longitudinal coefficients for hull dominated vessels.

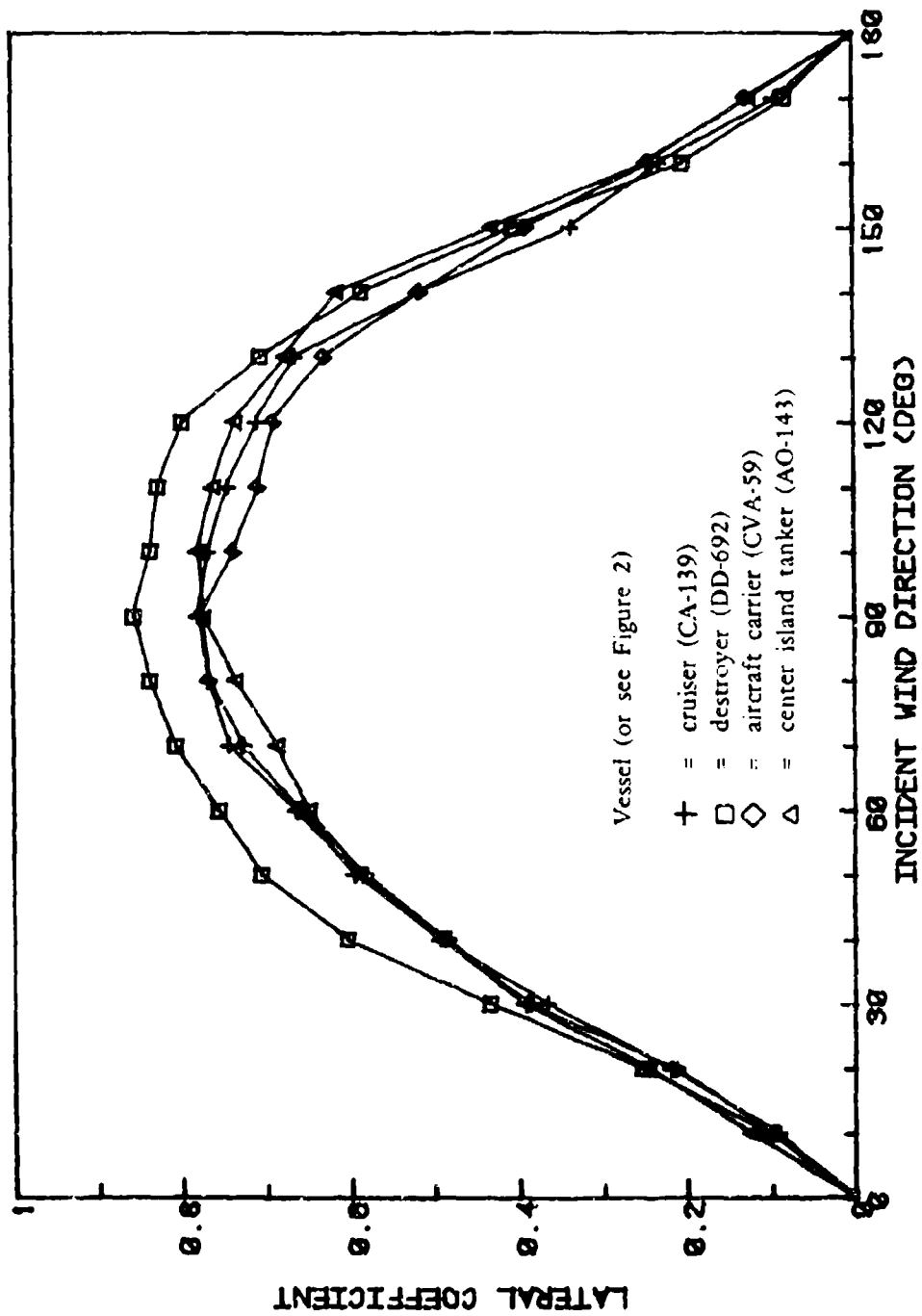


Figure 20. Representative lateral coefficients with sinusoidal shape functions.

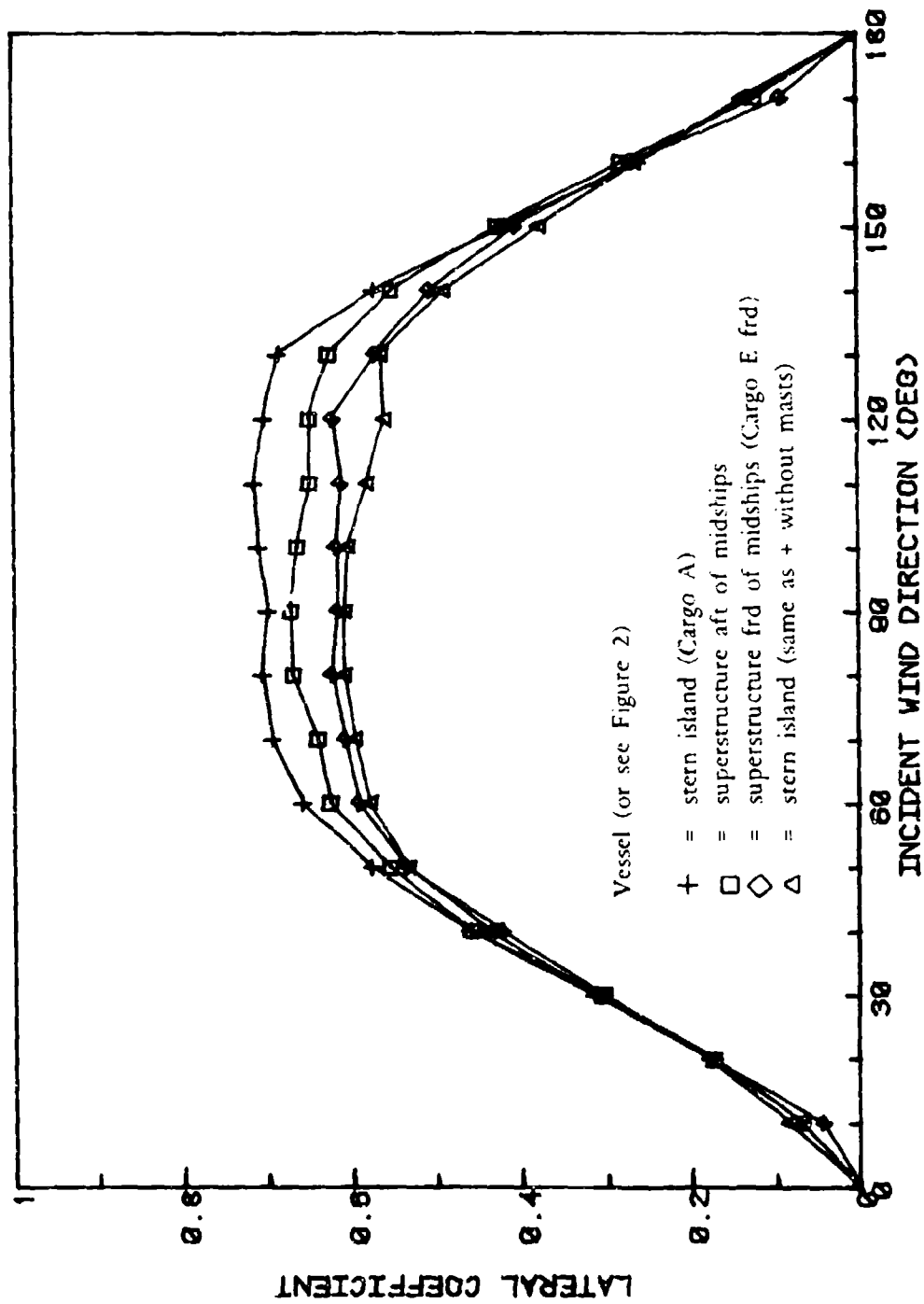


Figure 21. Representative lateral coefficients with flattened shape functions.

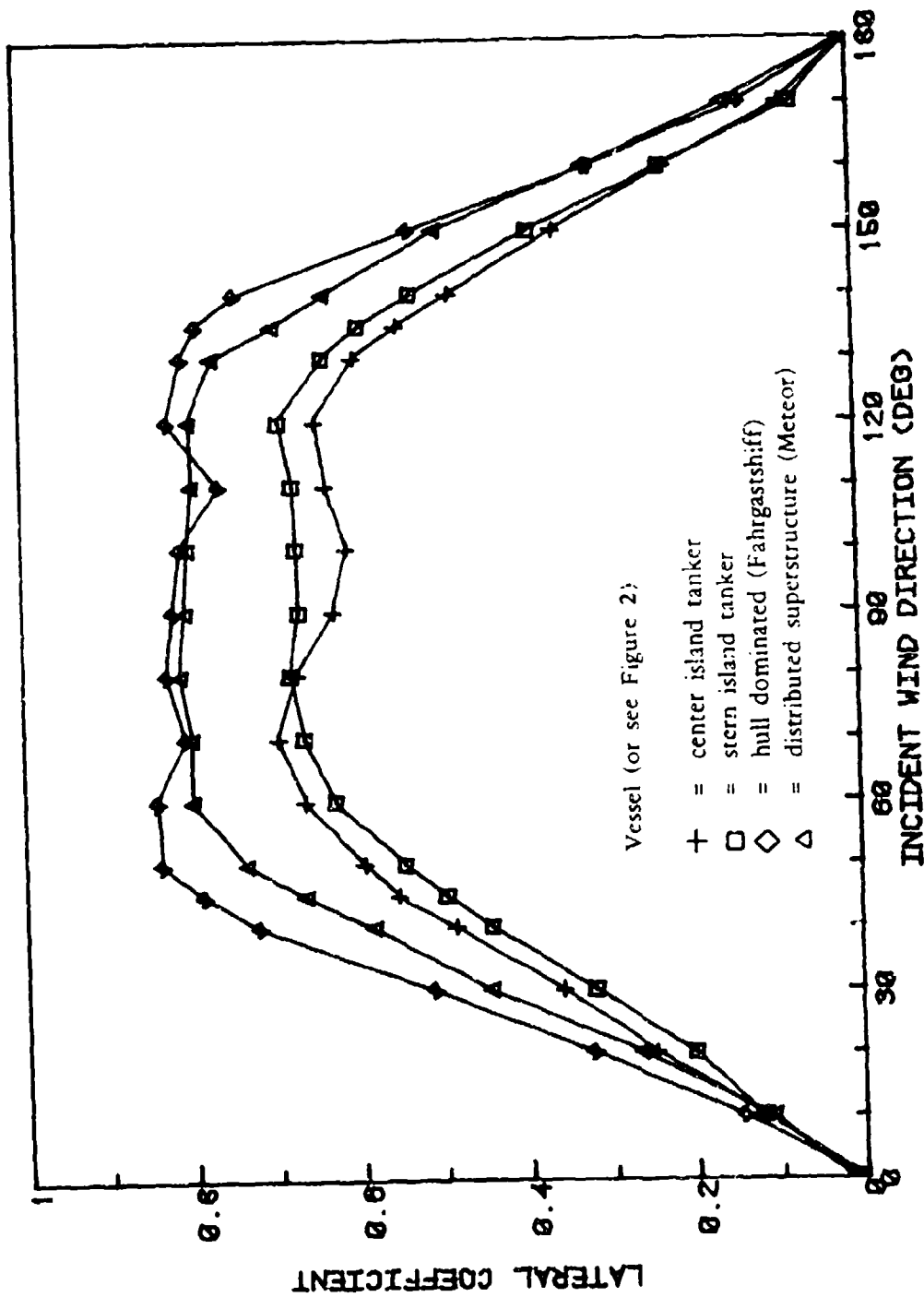


Figure 22. Representative lateral coefficients with extremely flattened shape functions.

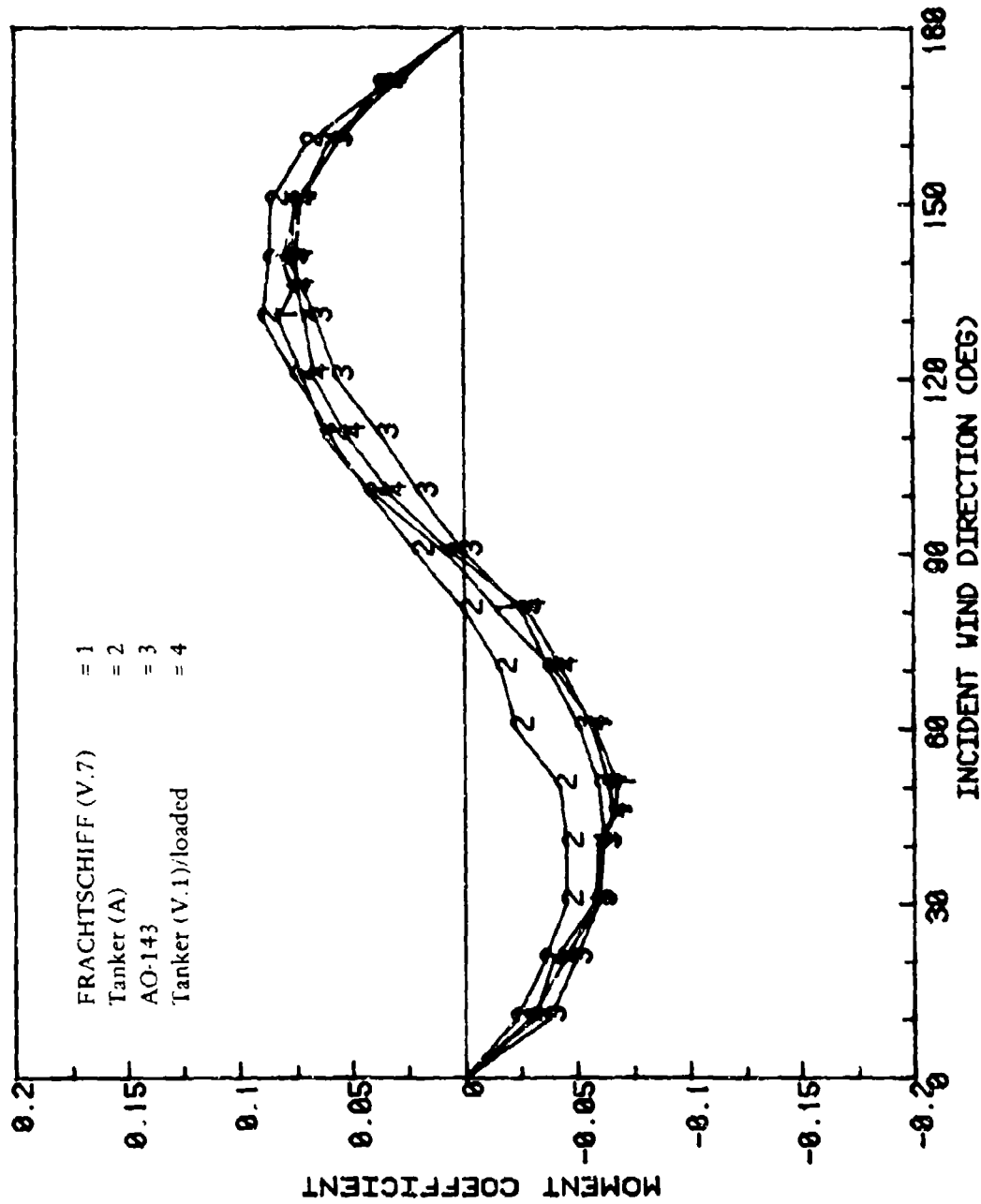


Figure 23. Experimental yaw moment coefficient for center island tankers.

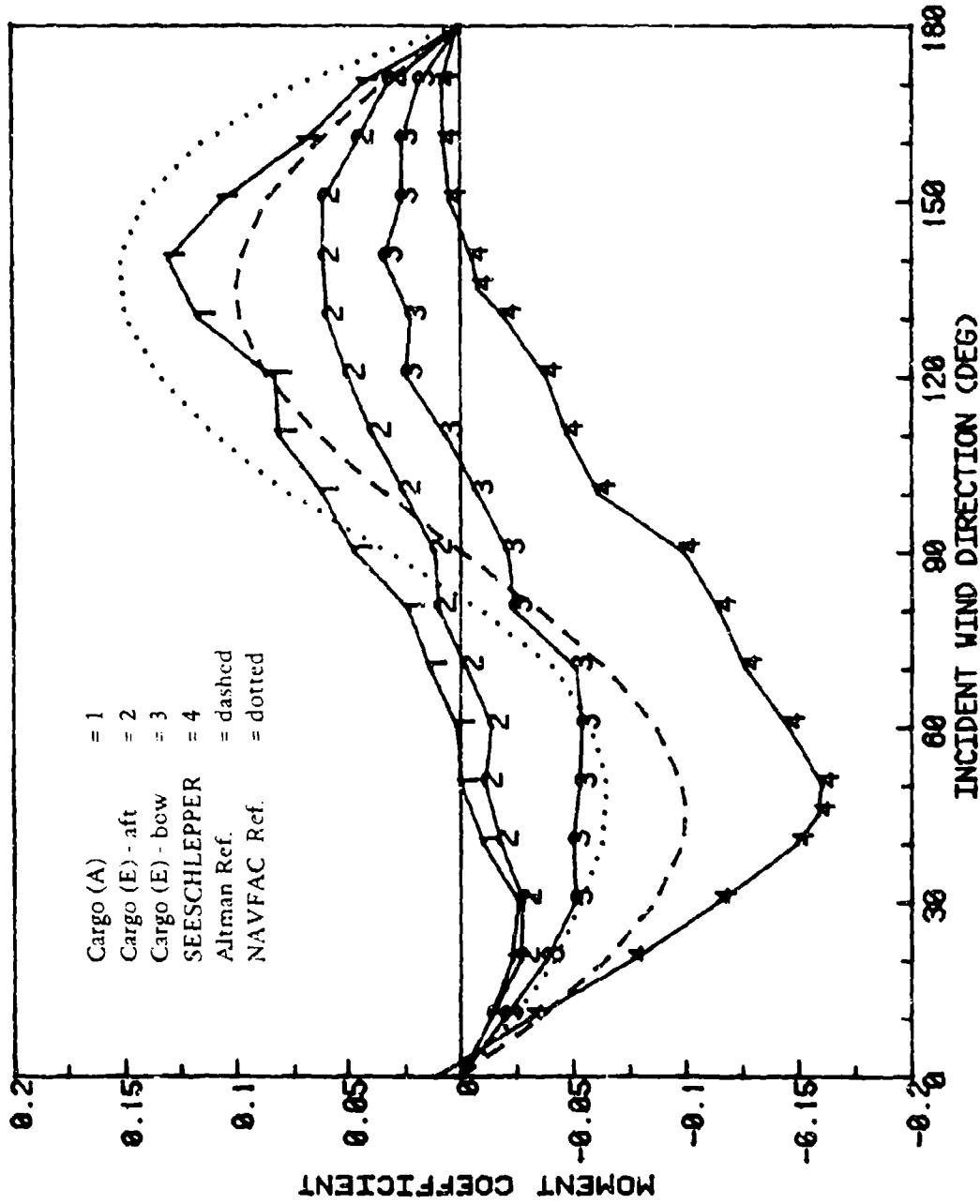


Figure 24. Sample experimental and recommended yaw moment coefficients (see Figure 4).

## Appendix

### SAMPLE PROBLEM

For demonstration purposes, the following example of the wind load determination for the center island tanker S. S. Pennsylvania (Figure A-1) is presented for an arbitrary 30 knot wind. Refer to the summary section for the expressions used in this example.



Figure A-1. S. S. Pennsylvania

Projected areas of vessel, as estimated from Figure A-1, and known vessel dimensions are:

$$A_Y = 19,390 \text{ ft}^2$$

$$A_H = 16,660 \text{ ft}^2$$

$$A_S = 2,730 \text{ ft}^2$$

$$A_X = 4,500 \text{ ft}^2$$

$$L = 595 \text{ ft}$$

Wind Gradient Approximations and  $C_Y$

Average height of freeboard = 14 ft (0 - 28 ft)

Average height of superstructure = 43 ft (28 - 57)

Normalized local wind speed is taken from the wind gradient curve (Figure 3), with  $n = 7$ :

$$0 \text{ to } 28 \text{ ft} \dots\dots\dots (\bar{V}_H/V_R)^2 \cong 0.60$$

$$28 \text{ to } 57 \text{ ft} \dots\dots\dots (\bar{V}_S/V_R)^2 \cong 1.11$$

Such that

$$C_{YM} = (0.92) \frac{(1.11)(2,730) + (0.60)(16,660)}{19,390} = 0.62$$

Thus, for the lateral force in a 30 knot wind, from Equation 1,

$$\begin{aligned} F_Y(\theta) &= \frac{1}{2} \rho A_Y V^2 C_{YM} f(\theta) \\ &= \frac{1}{2} (0.00237 \text{ lb-sec}^2/\text{ft}^4) (19,390 \text{ ft}^2) (30 \text{ kt})^2 \\ &\quad \cdot (1.688 \text{ ft/sec/kt})^2 (0.62) f(\theta) \end{aligned}$$

Substituting  $f(\theta)$  from Equation 3, or using Figure 4, lateral force

$$= (3.66 \times 10^4) \frac{\sin \theta - (\sin 5\theta)/20}{0.95} \quad (1b)$$

This lateral force is shown in Figure A-2, along with Reynold's Number-scaled experimental data. Since no information as to the ship's loading condition (and therefore projected areas) is available from the test report, the experimental data should be used only as a qualitative check on the general behavior of the calculated loads. The particular shape function recommended by this report is shown to be a good fit to the experimental data.

$C_{XS}$ . The initial mean longitudinal coefficient value is  $C_{XB} = 0.70$  ( $\pm 0.06$ ), but since the SS PENNSYLVANIA is a center island tanker with uncluttered decks, the coefficient is adjusted to  $C_{XB} = 0.70 + 0.10 = 0.80$

And, for center island tankers,

$$C_{XS} \sim 3/4 C_{XB} = 0.60; \theta_z \cong 100 \text{ degrees}$$

Such that, for  $\theta < \theta_z$

$$\begin{aligned} F_X(\theta) &= \frac{1}{2} \rho V^2 A_X C_X f(\psi)^+ \\ &= \frac{1}{2} (0.00237 \text{ lb-sec}^2/\text{ft}^4) (4,500 \text{ ft}^2) (30 \text{ kt})^2 \\ &\quad \cdot (1.688 \text{ ft/sec/kt})^2 (0.80) f(\psi)^+ \end{aligned}$$

Substituting for  $f(\psi)^+$  from Equations 6 and 7,

$$F_X(\theta) = (1.09 \times 10^4) \left( \frac{\sin \psi - (\sin 5\psi)/10}{0.9} \right) \quad (1b)$$

and

$$\psi = (0.9) \theta + 90$$

The longitudinal force for  $\theta > \theta_z$  is identical to the above equation, except  $C_{XS} = 0.60$  is used, and Equation 8 is used for  $\psi$ :

$$\psi = \frac{9}{8} \theta + 67.5$$

The longitudinal force for this tanker is illustrated in Figure A-3, along with Reynold's Number-scaled experimental data. Again, because the projected area of the model is unknown, only a qualitative check is possible. This shape function, with its "skewed" behavior around 100° and the flattened tails, shows the same characteristic behavior as the experimental results.

N. The recommended wind induced yaw moment coefficient,  $C_N(\theta)$ , for a trim center island tanker is shown in Figure 13. The moment is calculated using Equation 1:

$$\begin{aligned}
 N &= \frac{1}{2} \rho V^2 A_Y L C_N(\theta) \\
 &= \frac{1}{2} (0.0237 \text{ lb-sec}^2/\text{ft}^4) (30 \text{ kt})^2 (1.688 \text{ ft/sec/kt})^2 \\
 &\quad \cdot (19,380 \text{ ft}^2) (595 \text{ ft}) C_N(\theta) \\
 &= (3.5 \times 10^7) C_N(\theta) \text{ (ft-lb)}
 \end{aligned}$$

The moment is shown in Figure A-4, along with Reynold's Number-scaled experimental data.

The ship used in this example could be classified as a "center-balanced superstructure" ship, so the yaw moment coefficients recommended in Reference 1 and shown as dotted in Figure 16 could have been used instead of the specialized curves in Figure 13. A comparison of  $N(\theta)$  values between Figures 13 and 16 shows that this alternate function would have overestimated the measured minimum and maximum yaw moments by approximately 100%. This clearly demonstrates the potential errors of using a too simplistic loading function in the moment estimation.

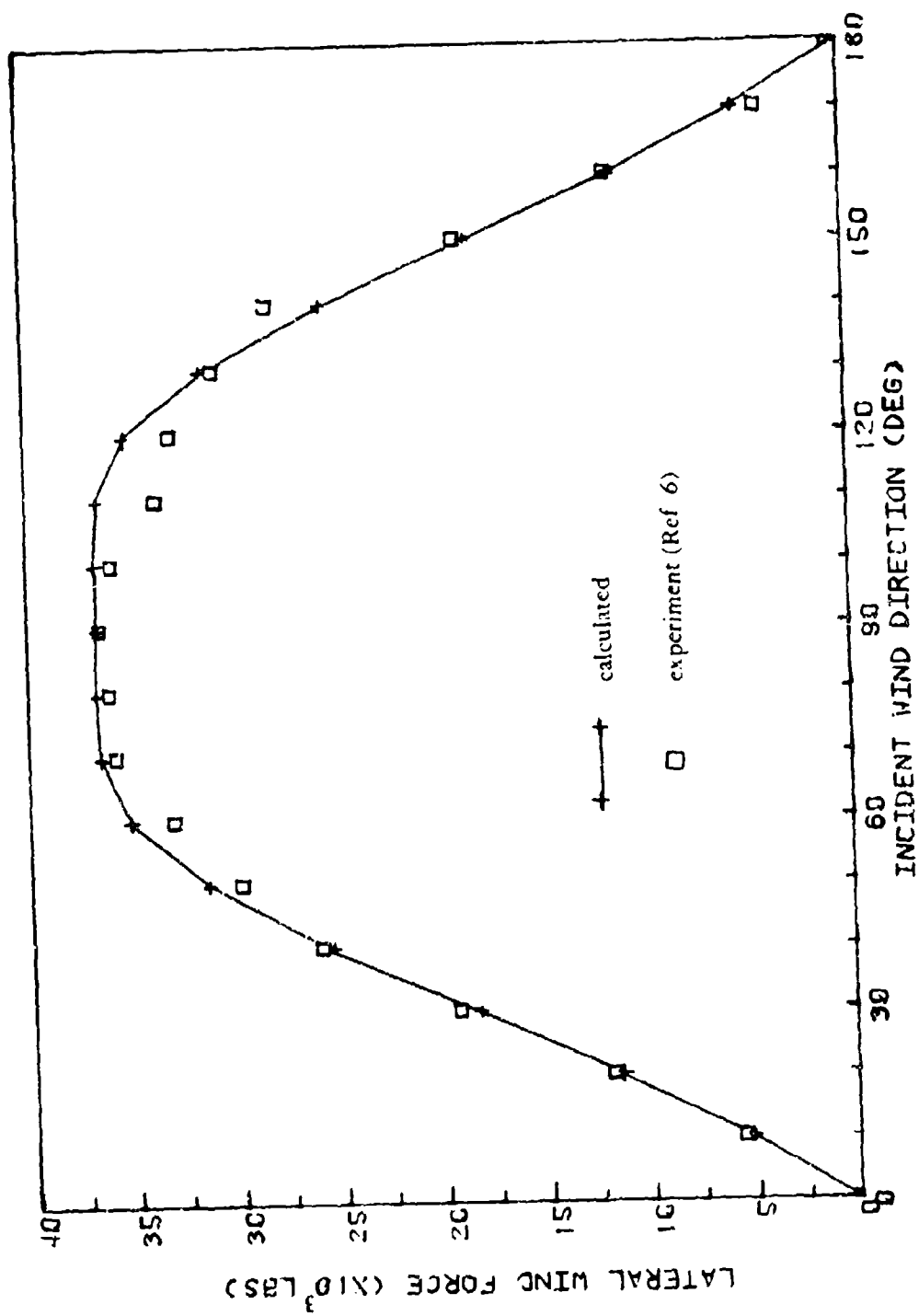


Figure A-2. Lateral wind loads for SS PENNSYLVANIA

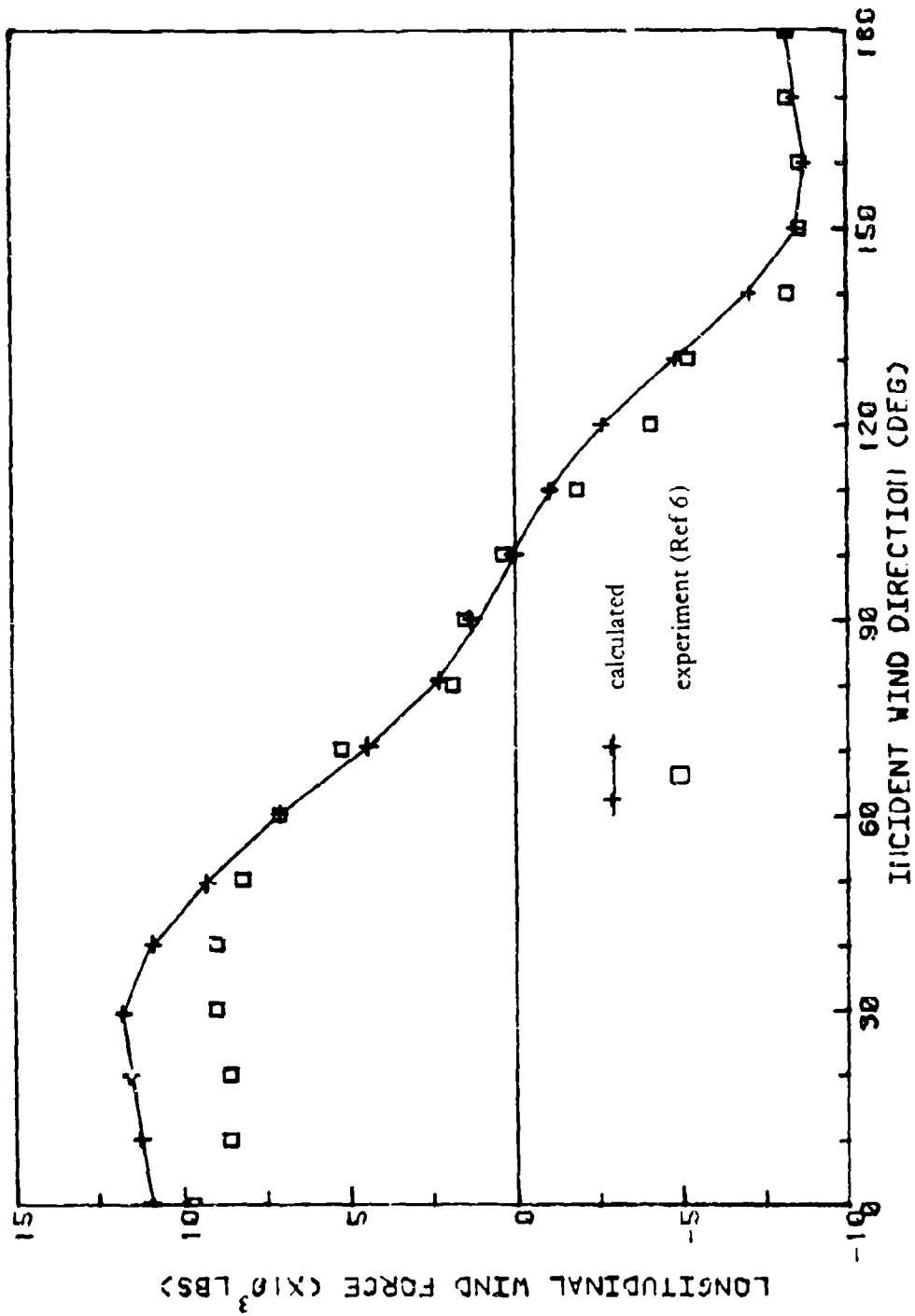


Figure A-3. Longitudinal wind loads for SS PENNSYLVANIA.

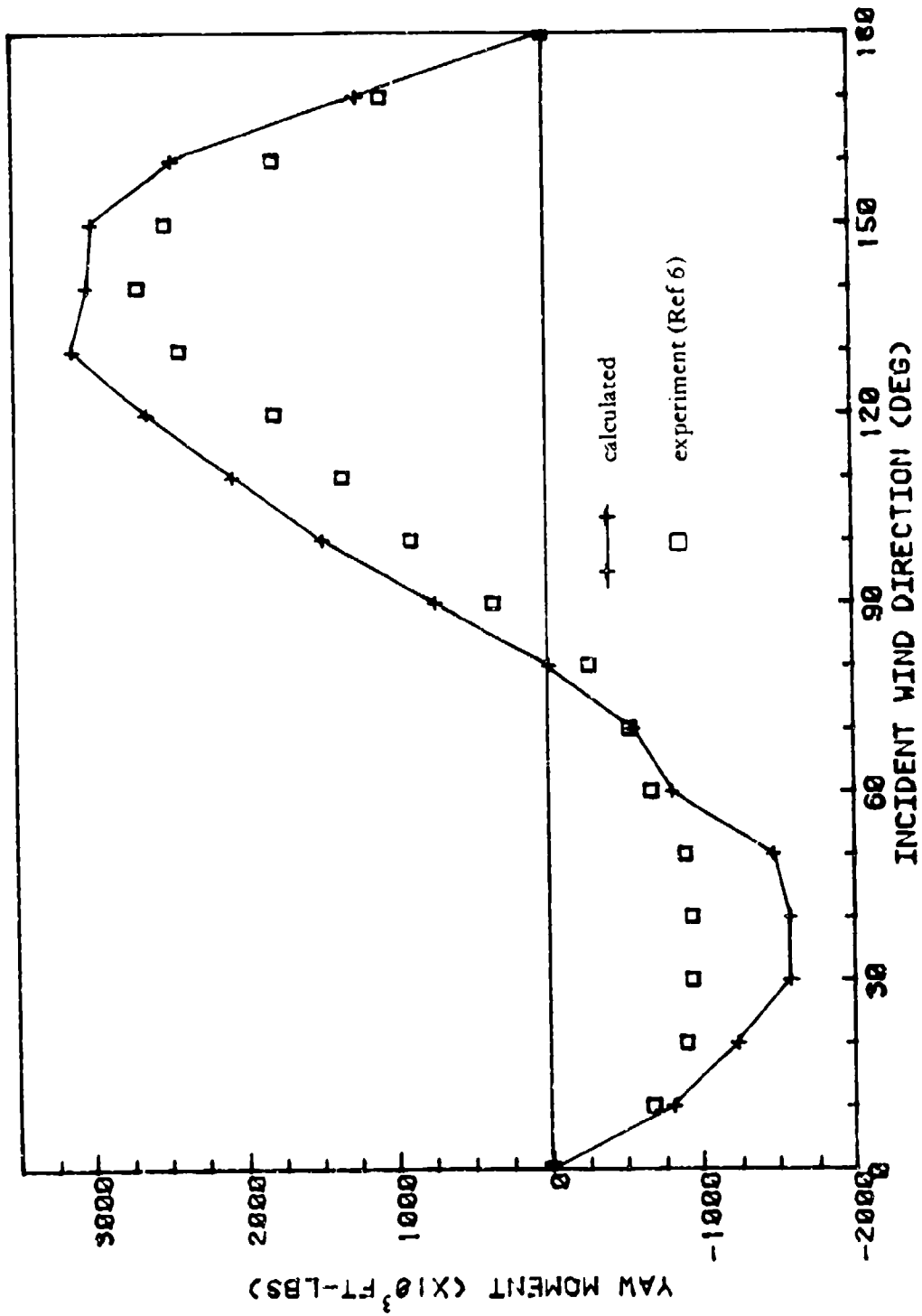


Figure A-4. Yaw wind moment for SS PENNSYLVANIA.

## DISTRIBUTION LIST

AFB CESCH, Wright-Patterson  
ARCTICSUBLAB Code 54, San Diego, CA  
ARMY BMDSC-RE (H. McClellan) Huntsville AL  
ARMY COASTAL ENGR RSCH CEN Fort Belvoir VA; R. Jachowski, Fort Belvoir VA  
ARMY COE Philadelphia Dist. (LIBRARY) Philadelphia, PA  
ARMY CORPS OF ENGINEERS MRD-Eng. Div., Omaha NE; Seattle Dist. Library, Seattle WA  
ARMY CRREL A. Kovacs, Hanover NH; Library, Hanover NH  
ARMY DARCOM Code DRCMM-CS Alexandria VA  
ARMY ENG WATERWAYS EXP STA Library, Vicksburg MS  
ARMY ENGR DIST. Library, Portland OR  
ARMY ENVIRON. HYGIENE AGCY HSE-EW Water Qual Eng Div Aberdeen Prov Grnd MD  
ARMY MATERIALS & MECHANICS RESEARCH CENTER Dr. Lenoe, Watertown MA  
ARMY TRANSPORTATION SCHOOL Code ATSP0 CD-TE Fort Eustis, VA  
ASST SECRETARY OF THE NAVY Spec. Assist Submarines, Washington DC  
BUREAU OF RECLAMATION Code 1512 (C. Selander) Denver CO  
CNM MAT-0718, Washington, DC; NMAT - 044, Washington DC  
CNO Code NOP-964, Washington DC; Code OP 323, Washington DC; Code OPNAV 09B24 (H); Code OPNAV  
22, Wash DC; Code OPNAV 23, Wash DC; OP-23 (Capt J.H. Howland) Washinton, DC; OP987J (J.  
Boosman), Pentagon  
COMNAVBEACHPHIBREFTRAGRU ONE San Diego CA  
COMSUBDEVGRUONE Operations Offr, San Diego, CA  
DEFENSE INTELLIGENCE AGENCY DB-4CI Washington DC  
DEFFUELSUPPCEN DFSC-OWE (Grafton) Alexandria, VA  
DTIC Defense Technical Info Ctr/Alexandria, VA  
HCU ONE CO, Bishops Point, HI  
LIBRARY OF CONGRESS Washington, DC (Sciences & Tech Div)  
MCAS Facil. Engr. Div. Cherry Point NC  
MILITARY SEALIFT COMMAND Washington DC  
NAF PWO, Atsugi Japan  
NALF OINC, San Diego, CA  
NARF Equipment Engineering Division (Code 61000), Pensacola, FL  
NAS Dir. Util. Div., Bermuda; PWD - Engr Div. Oak Harbor, WA; PWD Maint. Div., New Orleans, Belle  
Chasse LA; PWD, Code 1821H (Pfankuch) Miramar, SD CA; PWO Belle Chasse, LA; PWO Key West FL;  
PWO, Glenview IL; SCE Norfolk, VA; Shore Facil. Ofr Norfolk, VA  
NATL BUREAU OF STANDARDS Kovacs, Washington, D.C.  
NATL RESEARCH COUNCIL Naval Studies Board, Washington DC  
NAVACT PWO, London UK  
NAVAEROSPREGMEDCEN SCE, Pensacola FL  
NAVAIRDEVCCEN Code 813, Warminster PA  
NAVCOASTSYSTCTR CO, Panama City FL; Code 715 (J Quirk) Panama City, FL; Code 715 (J. Mittleman)  
Panama City, FL; Library Panama City, FL; PWO Panama City, FL  
NAVCOMMAREAMSTRSTA SCE Unit 1 Naples Italy  
NAVCOMMSTA Code 401 Nea Makri, Greece; PWD - Maint Control Div, Diego Garcia Is.; PWO, Exmouth,  
Australia  
NAVEDTRAPRODEVCCEN Technical Library, Pensacola, FL  
NAVELEXSYSCOM Code PME 124-61, Washington, DC; PME 124-612, Wash DC  
NAVEODFAC Code 605, Indian Head MD  
NAVFAC PWO, Centerville Bch, Ferndale CA  
NAVFACENGCOM Code 03T (Essoglou) Alexandria, VA; Code 043 Alexandria, VA; Code 044 Alexandria,  
VA; Code 0453 (D. Potter) Alexandria, VA; Code 0453C, Alexandria, VA; Code 04A1 Alexandria, VA;  
Code 100 Alexandria, VA; Code 1002B (J. Leimanis) Alexandria, VA; Code 1113 (T. Stevens) Alexandria,  
VA; Morrison Yap, Caroline Is.; ROICC Code 495 Portsmouth VA  
NAVFACENGCOM - CHES DIV. Code 407 (D Scheesele) Washington, DC; Code FPO-1C Washington DC;  
FPO-1 Washington, DC; FPO-IEA5 Washington DC  
NAVFACENGCOM - LANT DIV. Eur. BR Deputy Dir, Naples Italy; RDT&ELO 102, Norfolk VA  
NAVFACENGCOM - NORTH DIV. (Boretsky) Philadelphia, PA; CO; Code 04 Philadelphia, PA; Code 1028,  
RDT&ELO, Philadelphia PA; ROICC, Contracts, Crane IN  
NAVFACENGCOM - PAC DIV. CODE 09P PEARL HARBOR HI; Code 402, RDT&E, Pearl Harbor HI;  
Commander, Pearl Harbor, HI  
NAVFACENGCOM - SOUTH DIV. Code 90, RDT&ELO, Charleston SC  
NAVFACENGCOM - WEST DIV. Code 04B San Bruno, CA; O9P/20 San Bruno, CA; RDT&ELO Code 2011  
San Bruno, CA

NAVFACENCOM CONTRACT Eng Div dir, Southwest Pac, Manila, PI; OICC, Southwest Pac, Manila, PI;  
 OICC/ROICC, Balboa Panama Canal; ROICC, NAS, Corpus Christi, TX  
 NAVOCEANO Library Bay St. Louis, MS  
 NAVOCEANSYSCEN Code 41, San Diego, CA; Code 4473 Bayside Library, San Diego, CA; Code 4473B  
 (Tech Lib) San Diego, CA; Code 52 (H. Talkington) San Diego CA; Code 5204 (J. Stachiw), San Diego,  
 CA; Code 5214 (H. Wheeler), San Diego CA; Code 5221 (R. Jones) San Diego CA; Code 5311 (Bachman)  
 San Diego, CA; Hawaii Lab (R Yumori) Kailua, HI; Hi Lab Tech Lib Kailua HI  
 NAVPGSCOL C. Morers Monterey CA; E. Thornton, Monterey CA  
 NAVPHIBASE CO, ACB 2 Norfolk, VA; COMNAVBEACHGRU TWO Norfolk VA; Code S3T, Norfolk VA;  
 Harbor Clearance Unit Two, Little Creek, VA; SCE, Coronado, San Diego CA  
 NAVREGMEDCEN SCE (D. Kaye)  
 NAVSEASYSYSCOM Code PMS 395 A 3, Washington, DC; Code SEA OOC Washington, DC  
 NAVSHIPREFAC Library, Guam; SCE Subic Bay  
 NAVSHIPYD Bremerton, WA (Carr Inlet Acoustic Range); Code 202.4, Long Beach CA; Code 440  
 Portsmouth NH; Code 440, Puget Sound, Bremerton WA; Tech Library, Vallejo, CA  
 NAVSTA CO Roosevelt Roads P.R. Puerto Rico; Dir Engr Div, PWD, Mayport FL; PWD (LTJG.P.M.  
 Motolenich), Puerto Rico; PWO Pearl Harbor, HI; PWO, Keflavik Iceland; PWO, Mayport FL; SCE, Guam;  
 SCE, Subic Bay, R.P.; Security Offr, San Francisco, CA  
 NAVTECHTRACEN SCE, Pensacola FL  
 NAVWPNCEN Code 3803 China Lake, CA  
 NAVWPNSTA Code 092, Colts Neck NJ  
 NAVWPNSTA PW Office Yorktown, VA  
 NAVWPNSTA PWD - Maint. Control Div., Concord, CA; PWD - Supr Gen Engr, Seal Beach, CA; PWO,  
 Charleston, SC; PWO, Seal Beach CA  
 NAVWPNSUPPCEN Code 09 Crane IN  
 NCBC Code 10 Davisville, RI; Code 15, Port Hueneme CA; Code 155, Port Hueneme CA; Code 156, Port  
 Hueneme, CA  
 NMCB FIVE, Operations Dept  
 NOAA (Dr. T. Mc Guinness) Rockville, MD; Library Rockville, MD  
 NORDA Code 410 Bay St. Louis, MS; Code 440 (Ocean Rsch Off) Bay St. Louis MS  
 NRL Code 5800 Washington, DC; Code 5843 (F. Rosenthal) Washington, DC; Code 8441 (R.A. Skop),  
 Washington DC  
 NROTC J.W. Stephenson, UC, Berkeley, CA  
 NSD SCE, Subic Bay, R.P.  
 NUCLEAR REGULATORY COMMISSION T.C. Johnson, Washington, DC  
 NUSC Code 131 New London, CT; Code 332, B-80 (J. Wilcox) New London, CT; Code EA123 (R.S. Munn),  
 New London CT; Code TA131 (G. De la Cruz), New London CT  
 ONR (Scientific Dir) Pasadena, CA; Central Regional Office, Boston, MA; Code 481, Bay St. Louis, MS;  
 Code 485 (Silva) Arlington, VA; Code 700F Arlington VA  
 PHIBCB 1 P&E, San Diego, CA; 1, CO San Diego, CA  
 PMTC Code 3331 (S. Opatowsky) Point Mugu, CA; EOD Mobile Unit, Point Mugu, CA; Pat. Counsel, Point  
 Mugu CA  
 PWC CO Norfolk, VA; CO, (Code 10), Oakland, CA; CO, Great Lakes IL; CO, Pearl Harbor HI; Code 10,  
 Great Lakes, IL; Code 120, Oakland CA; Code 120C, (Library) San Diego, CA; Code 128, Guam; Code  
 154, Great Lakes, IL; Code 200, Great Lakes IL; Code 30C, Norfolk, VA; Code 30C, San Diego, CA; Code  
 400, Great Lakes, IL; Code 400, Pearl Harbor, HI; Code 400, San Diego, CA; Code 420, Great Lakes, IL;  
 Code 420, Oakland, CA; Code 700, San Diego, CA  
 UCT ONE OIC, Norfolk, VA; UCT TWO OIC, Port Hueneme CA  
 US DEPT OF INTERIOR Bur of Land Mngmnt Code 583 (T F Sullivan) Washington, DC  
 US GEOLOGICAL SURVEY Off. Marine Geology, Piteleki, Reston VA  
 US NAVAL FORCES Korea (ENJ-P&O)  
 USCG (Smith), Washington, DC; G-EOE-4 (T Dowd), Washington, DC  
 USCG R&D CENTER CO Groton, CT; D. Motherway, Groton CT  
 USDA Forest Service, San Dimas, CA  
 USNA Civil Engr Dept (R. Erchyl) Annapolis MD; Ocean Sys. Eng Dept (Dr. Monney) Annapolis, MD; PWD  
 Engr. Div. (C. Bradford) Annapolis MD